

# $H \rightarrow \tau^+\tau^-$ branching ratio study at $\sqrt{s} = 250$ GeV at the ILC with the ILD detector

Shin-ichi Kawada<sup>1,†</sup>, Keisuke Fujii<sup>2</sup>, Taikan Suehara<sup>3</sup>,  
Tohru Takahashi<sup>1</sup>, Tomohiko Tanabe<sup>3</sup>

February 2, 2013 (revised at March 22, 2013)

1: Advanced Sciences of Matter (AdSM), Hiroshima University, 1-3-1, Kagamiyama, Higashi-Hiroshima, Hiroshima, 739-8530, Japan  
2: High Energy Accelerator Research Organization (KEK), 1-1, Oho, Tsukuba, Ibaraki, 305-0801, Japan  
3: International Center for Elementary Particle Physics (ICEPP), The University of Tokyo, 7-3-1, Hongo, Bunkyo-ku, Tokyo, 113-0033, Japan

† : [s-kawada@huhep.org](mailto:s-kawada@huhep.org)

## Abstract

We evaluated the measurement accuracy of the branching ratio of  $H \rightarrow \tau^+\tau^-$  mode at  $\sqrt{s} = 250$  GeV at the ILC with the ILD detector. We assumed the Higgs mass  $M_H = 120$  GeV, branching ratio  $\text{Br}(H \rightarrow \tau^+\tau^-) = 8.0\%$ , beam polarization  $P(e^-, e^+) = (-0.8, +0.3)$ , and integrated luminosity  $\int L dt = 250 \text{ fb}^{-1}$ . We used the LOI samples as the Monte-Carlo samples. The evaluation was performed by the ILD full detector simulation. All Standard Model backgrounds were included in this study. We obtained the accuracy  $\Delta(\sigma \cdot \text{Br})/(\sigma \cdot \text{Br}) = 3.5\%$ . The scaled result to  $M_H = 125$  GeV is calculated to be 4.2 %.

## 1 Introduction

A new Higgs-like particle was discovered by the ATLAS and the CMS experiments [1, 2]. One of the next important themes for particle physics is the investigation of that new particle, especially the mass generation mechanism.

One of the important properties of Higgs boson is its branching ratio. In the Standard Model (SM) of particle physics, the Yukawa coupling constant of matter fermions with the Higgs boson is proportional to the fermion mass. Besides, if there is new physics, the coupling constant may deviate from the SM prediction. Therefore, the branching ratio is a probe for new physics.

In this note, we focus on the branching ratio of  $H \rightarrow \tau^+\tau^-$  mode. We estimate the measurement accuracy of the  $H \rightarrow \tau^+\tau^-$  branching ratio at  $\sqrt{s} = 250$  GeV with the ILD full detector simulation.

## 2 Signal and Background

The main Higgs production process at  $\sqrt{s} = 250$  GeV is the Higgs-strahlung process ( $e^+e^- \rightarrow ZH$ ). There are three types of signal depending on the decay of the  $Z$  boson, as shown in Figure 1. In this note, we concentrate on (A)  $Z \rightarrow l^+l^-$  mode and (B)  $Z \rightarrow q\bar{q}$  mode.

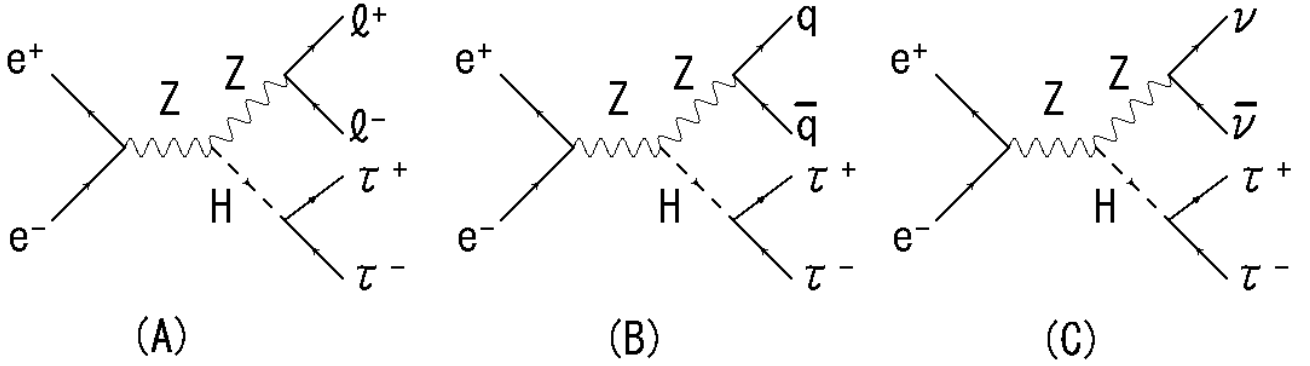


Figure 1: The diagrams of signal processes. (A):  $Z \rightarrow l^+l^-$  mode, (B):  $Z \rightarrow q\bar{q}$  mode, (C):  $Z \rightarrow \nu\bar{\nu}$  mode.

The  $Z \rightarrow \nu\bar{\nu}$  mode has been found to contribute negligibly to the overall precision which is dominated by the  $Z \rightarrow q\bar{q}$  mode. However, at higher center-of-mass energies, the  $e^+e^- \rightarrow \nu\bar{\nu}H$  mode is expected to contribute substantially due to the increase in the cross section of  $WW$  fusion process.

## 2.1 $Z \rightarrow l^+l^-$ mode

In this mode, we only considered  $Z \rightarrow e^+e^-$  mode and  $Z \rightarrow \mu^+\mu^-$  mode as the signal process. The signal cross section of this mode is 1.9 fb. The dominant background processes are the four leptons processes ( $e^+e^- \rightarrow eeee$ ,  $ee\mu\mu$ ,  $ee\tau\tau$ ,  $\mu\mu\mu\mu$ ,  $\mu\mu\tau\tau$ , and  $\tau\tau\tau\tau$ ). An example diagram is shown in Figure 2-(A). Other background processes are  $e^+e^- \rightarrow ZH$  reactions where the Higgs boson does not decay to tau pairs.

## 2.2 $Z \rightarrow q\bar{q}$ mode

The signal cross section of this mode is 19.8 fb. The possible background processes for this mode are  $qqqq$ ,  $qql\bar{l}$ , and  $qql\nu$ , which come from  $e^+e^- \rightarrow W^+W^-$  or  $e^+e^- \rightarrow ZZ$  reactions. An example diagram is shown in Figure 2-(B). Other possible backgrounds are  $e^+e^- \rightarrow ZH$  with  $Z \rightarrow \tau^+\tau^-$  and  $H \rightarrow q\bar{q}$ . These processes have the same final state to the signal.

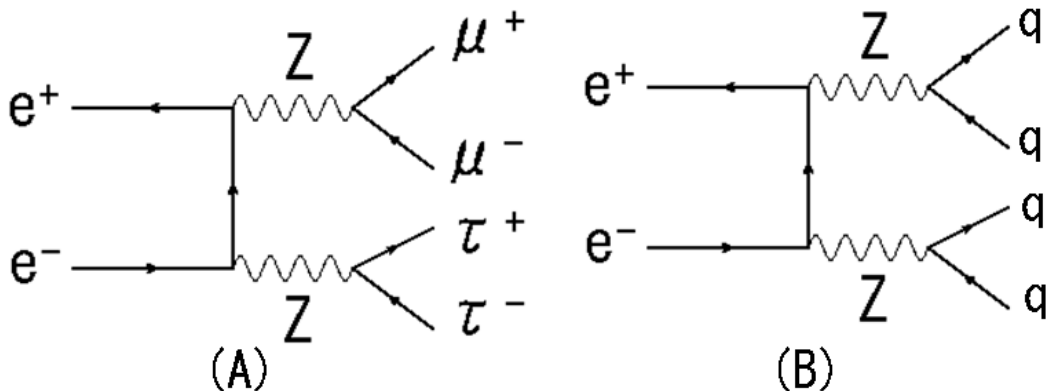


Figure 2: Example diagrams of possible background. (A):  $\mu\mu\tau\tau$  background for  $Z \rightarrow l^+l^-$  mode, (B):  $qqqq$  background for  $Z \rightarrow q\bar{q}$  mode.

### 3 Simulation Conditions

We performed the detector simulation with Mokka [3], a Geant4-based [4] full simulation, with the ILD\_00 detector model. TAUOLA [5] was used for the tau decay simulation. The ILD\_00 detector model consists of vertex detector, time projection chamber, electromagnetic calorimeter (ECAL), hadronic calorimeter (HCAL), and yoke.

We used the signal and background samples which were generated in the context of the Letter of Intent [6]. The assumed center-of-mass energy is 250 GeV. The effects of beamstrahlung and initial state radiation are included. All Monte-Carlo sample information (process ID, process, polarization, cross section, number of events, and luminosity) are summarized in Tables 6 (page 9) and 7 (page 10). We assumed the Higgs mass  $M_H = 120$  GeV, branching ratio  $\text{Br}(H \rightarrow \tau^+\tau^-) = 8.0\%$  as assumed by PYTHIA [8], integrated luminosity  $\int L dt = 250 \text{ fb}^{-1}$ , and beam polarization  $P(e^+, e^-) = (+0.3, -0.8)$ . We also rescale the final result to the case of  $M_H = 125$  GeV and the  $H \rightarrow \tau^+\tau^-$  branching ratio which includes the NNLO corrections [9].

### 4 Event Reconstruction and Event Selection

#### 4.1 $Z \rightarrow l^+l^-$ mode

In this mode, we take the strategy of reconstructing the  $Z$  boson first, followed by the reconstruction of the tau pairs from the Higgs decay.

We applied lepton identification at first for dividing  $Z \rightarrow e^+e^-$  events and  $Z \rightarrow \mu^+\mu^-$  events by using the information of energy deposit in the calorimeter ( $E_{\text{ECAL}}$  and  $E_{\text{HCAL}}$ , where  $E_{\text{ECAL}}$  is the energy deposit in ECAL,  $E_{\text{HCAL}}$  is the energy deposit in HCAL, respectively) and track momentum ( $P_{\text{track}}$ ). Figures 3 - 6 are the plots of  $E_{\text{ECAL}}/(E_{\text{ECAL}} + E_{\text{HCAL}})$  and  $(E_{\text{ECAL}} + E_{\text{HCAL}})/P_{\text{track}}$ .

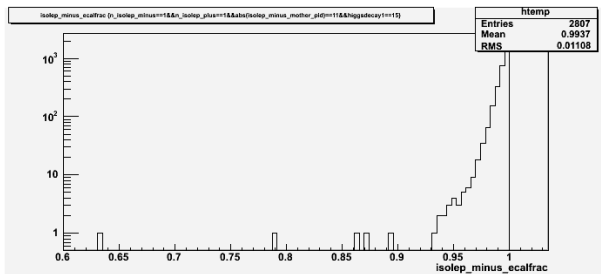


Figure 3: The plot of  $E_{\text{ECAL}}/(E_{\text{ECAL}} + E_{\text{HCAL}})$  for the  $e$  in  $eeH$  samples.

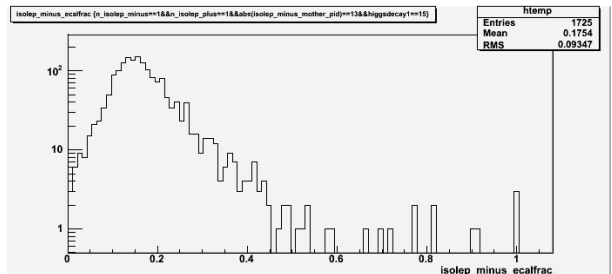


Figure 4: The plot of  $E_{\text{ECAL}}/(E_{\text{ECAL}} + E_{\text{HCAL}})$  for the  $\mu$  in  $\mu\mu H$  samples.

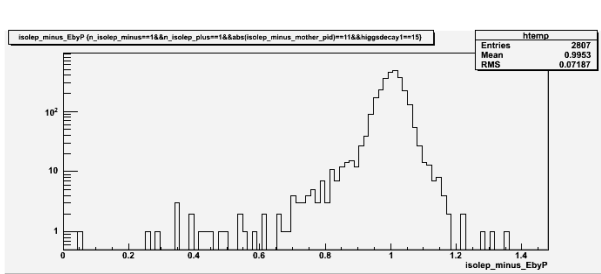


Figure 5: The plot of  $(E_{\text{ECAL}} + E_{\text{HCAL}})/P_{\text{track}}$  for the  $e$  in  $eeH$  samples.

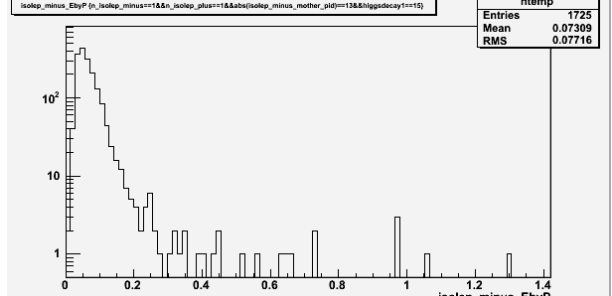


Figure 6: The plot of  $(E_{\text{ECAL}} + E_{\text{HCAL}})/P_{\text{track}}$  for the  $\mu$  in  $\mu\mu H$  samples.

From these plots, we define the criteria for lepton identification. The criteria for electron identification ( $e$ -ID) are:  $E_{\text{ECAL}}/(E_{\text{ECAL}} + E_{\text{HCAL}}) > 0.92$  and  $(E_{\text{ECAL}} + E_{\text{HCAL}})/P_{\text{track}} > 0.5$ . The criteria for muon identification ( $\mu$ -ID) are:  $E_{\text{ECAL}}/(E_{\text{ECAL}} + E_{\text{HCAL}}) < 0.6$  and  $(E_{\text{ECAL}} + E_{\text{HCAL}})/P_{\text{track}} < 0.5$ .

After the lepton identification, we applied selections to remove secondary leptons from tau decays. The strategy of this selection is to remove tracks which do not come from the interaction point (IP) by using the track energy  $E_{\text{track}}$  and impact parameter in the transverse direction  $d_0$  and longitudinal direction  $z_0$  with respect to the beam axis. Figures 7 - 12 show the  $|d_0/\sigma(d_0)|$ ,  $|z_0/\sigma(z_0)|$ , and  $E_{\text{track}}$  plots which through the lepton identification. We defined the tau rejection cut for the objects through the  $e$ -ID:  $|d_0/\sigma(d_0)| < 50$ ,  $|z_0/\sigma(z_0)| < 5$ , and  $E_{\text{track}} > 10$  GeV, and for the objects through the  $\mu$ -ID:  $|d_0/\sigma(d_0)| < 3$ ,  $|z_0/\sigma(z_0)| < 7$ , and  $E_{\text{track}} > 20$  GeV.

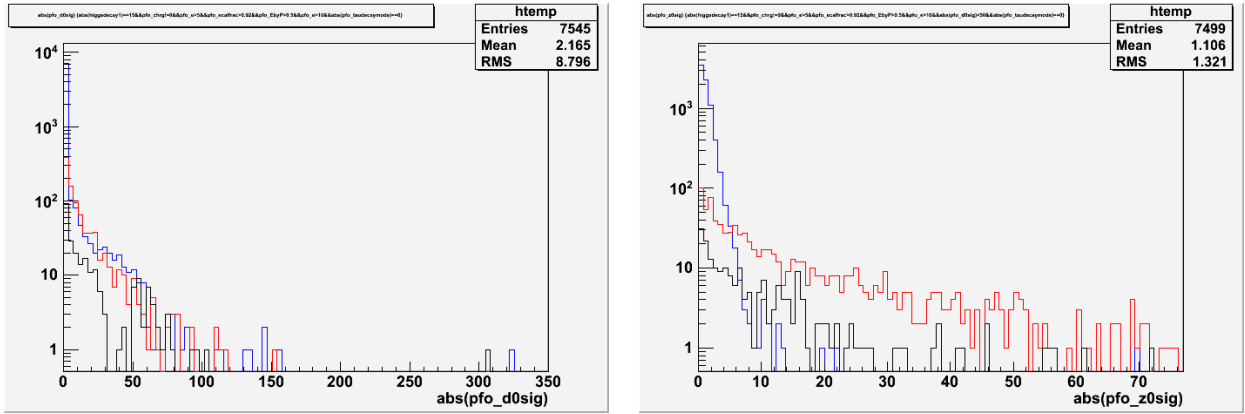


Figure 7: The plot of  $|d_0/\sigma(d_0)|$  of  $e$  of  $eeH$  process. Blue, red, and black histograms show the  $e$  from  $Z \rightarrow e^+e^-$ , the  $e$  from  $\tau \rightarrow e\nu\nu$ , and the hadrons from  $\tau$  decay, respectively.

Figure 8: The plot of  $|z_0/\sigma(z_0)|$  of  $e$  of  $eeH$  process. Blue, red, and black histograms show the  $e$  from  $Z \rightarrow e^+e^-$ , the  $e$  from  $\tau \rightarrow e\nu\nu$ , and the hadrons from  $\tau$  decay, respectively.

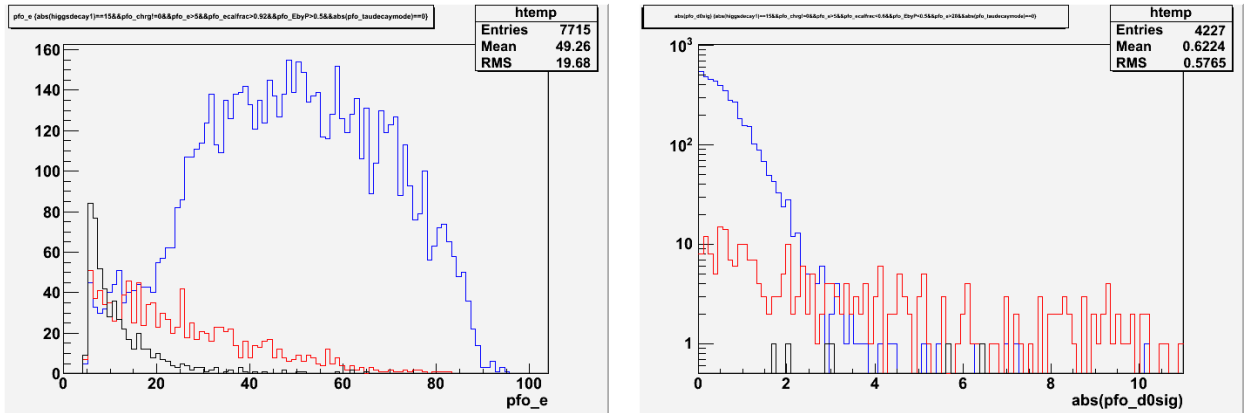


Figure 9: The plot of  $E_{\text{track}}$  of  $e$  of  $eeH$  process. Blue, red, and black histograms show the  $e$  from  $Z \rightarrow e^+e^-$ , the  $e$  from  $\tau \rightarrow e\nu\nu$ , and the hadrons from  $\tau$  decay, respectively.

Figure 10: The plot of  $|d_0/\sigma(d_0)|$  of  $\mu$  of  $\mu\mu H$  process. Blue, red, and black histograms show the  $\mu$  from  $Z \rightarrow \mu^+\mu^-$ , the  $\mu$  from  $\tau \rightarrow \mu\nu\nu$ , and the hadrons from  $\tau$  decay, respectively.

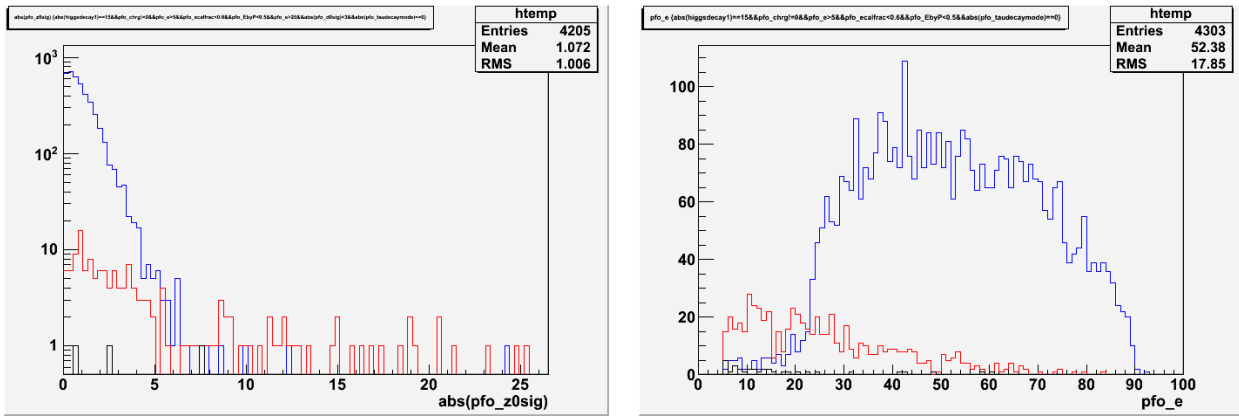


Figure 11: The plot of  $|z_0/\sigma(z_0)|$  of  $\mu$  of  $\mu\mu H$  process. Blue, red, and black histograms show the  $\mu$  from  $Z \rightarrow \mu^+\mu^-$ , the  $\mu$  from  $\tau \rightarrow \mu\nu\nu$ ,  $\mu$  from  $Z \rightarrow \mu^+\mu^-$ , the  $\mu$  from  $\tau \rightarrow \mu\nu\nu$ , and the hadrons from  $\tau$  decay, respectively.

Figure 12: The plot of  $E_{\text{track}}$  of  $\mu$  of  $\mu\mu H$  process. Blue, red, and black histograms show the  $\mu$  from  $Z \rightarrow \mu^+\mu^-$ , the  $\mu$  from  $\tau \rightarrow \mu\nu\nu$ ,  $\mu$  from  $Z \rightarrow \mu^+\mu^-$ , the  $\mu$  from  $\tau \rightarrow \mu\nu\nu$ , and the hadrons from  $\tau$  decay, respectively.

We applied the energy recovery procedure to correct for bremsstrahlung and final state radiation. In order to reconstruct the original  $Z$  boson, we have to use both the charged particles and the radiated photons. To achieve this, we defined the cone as shown in Figure 13. The four-momenta of the neutral particles in the cone were combined with that of the lepton candidate. We defined the half-opening angle of the cone with  $\cos \theta_{\text{cone}} = 0.999$  and applied the recovery procedure to the lepton candidates. The results are shown in Figures 14 and 15.

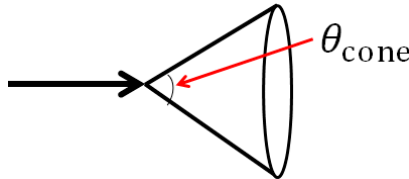


Figure 13: The definition of the cone. Black arrow shows the lepton candidate.  $\theta_{\text{cone}}$  is the angle of the cone.

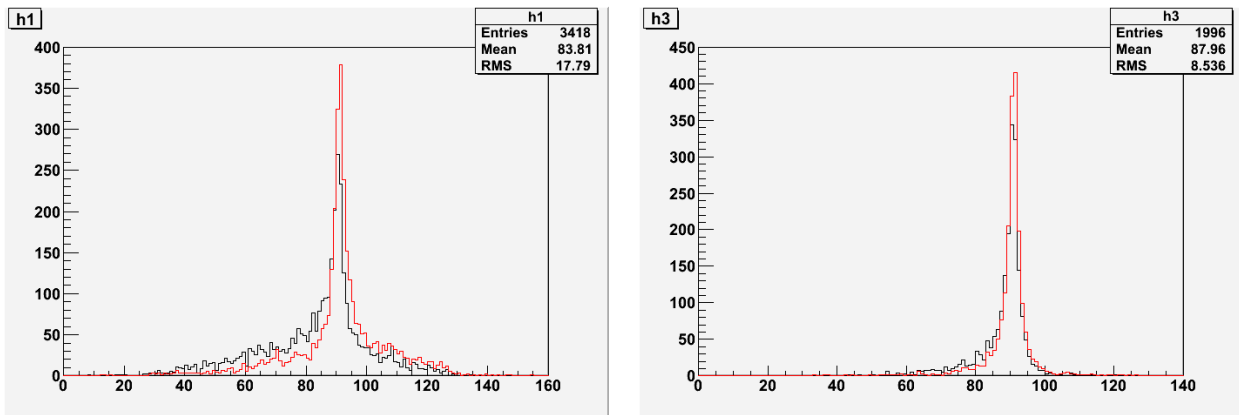


Figure 14: The results of recovery for  $Z \rightarrow e^+e^-$  mode. The horizontal axis shows the  $M_Z$ . Black and red histograms show the results of without recovery and with recovery ( $\cos \theta_{\text{cone}} = 0.999$ ), respectively.

Figure 15: The results of recovery for  $Z \rightarrow \mu^+\mu^-$  mode. The horizontal axis shows the  $M_Z$ . Black and red histograms show the results of without recovery and with recovery ( $\cos \theta_{\text{cone}} = 0.999$ ), respectively.

After that, we applied the tau finder to the remaining objects to reconstruct tau leptons. First of all, the objects which already used at  $Z$  boson reconstruction were rejected from tau reconstruction analysis. Then we search the highest energy track from the remaining objects, and combine the neighboring particles (which satisfies the angle with respect to the highest energy track less than 1.0 radian) with the combined mass less than 2 GeV. We regarded the combined object as a tau candidate. Then repeat these processes until there are no charged particles.

After finishing the event reconstruction, we applied the cuts for selecting signal, rejecting background. Before optimizing the cuts, we applied the preselection as follows for  $Z \rightarrow e^+e^-$  mode: number of  $e^+$  and  $e^- = 1$ , number of  $\tau^+$  and  $\tau^- = 1$ , and for  $Z \rightarrow \mu^+\mu^-$  mode: number of  $\mu^+$  and  $\mu^- = 1$ , number of  $\tau^+$  and  $\tau^- = 1$ .

We applied the following cuts for  $Z \rightarrow e^+e^-$  mode: number of tracks  $\leq 8$ ,  $115 \text{ GeV} < E_{\text{vis}} < 230 \text{ GeV}$ ,  $|\cos \theta_{\text{miss}}| < 0.99$ ,  $81 \text{ GeV} < M_Z < 113 \text{ GeV}$ ,  $\cos \theta_{e^-} < 0.92$ ,  $\cos \theta_{e^+} > -0.92$ ,  $E_{e^-} < 90 \text{ GeV}$ ,  $E_{e^+} < 90 \text{ GeV}$ ,  $\cos \theta_{\tau^+\tau^-} < -0.45$ ,  $\cos \theta_{\tau^-} < 0.92$ ,  $\cos \theta_{\tau^+} > -0.92$ , and  $116 \text{ GeV} < M_{\text{recoil}} < 142 \text{ GeV}$ , where  $E_{\text{vis}}$  is the visible energy,  $\theta_{\text{miss}}$  is the missing momentum angle with respect to beam axis,  $\theta_{e^-(e^+)}$  is the  $e^-(e^+)$  angle with respect to beam axis,  $E_{e^-(e^+)}$  is the  $e^-(e^+)$  energy,  $\theta_{\tau^+\tau^-}$  is the angle between  $\tau^+$  and  $\tau^-$ ,  $\theta_{\tau^-(\tau^+)}$  is the  $\tau^-(\tau^+)$  angle with respect to beam axis, and  $M_{\text{recoil}}$  is the recoil mass, respectively. The histograms of all cut variables are shown in Figures 17 - 28 (page 11 - 12). Table 1 shows the cut statistics of this mode. After the cuts, the  $Z \rightarrow e^+e^-$  signal events of 108.9 and background events of 76.0 remained. The statistical significance was calculated to be  $S/\sqrt{S+B} = 108.9/\sqrt{108.9+76.0} = 8.0\sigma$ .

We applied the following cuts for  $Z \rightarrow \mu^+\mu^-$  mode: number of tracks  $\leq 8$ ,  $115 \text{ GeV} < E_{\text{vis}} < 235 \text{ GeV}$ ,  $|\cos \theta_{\text{miss}}| < 0.98$ ,  $72 \text{ GeV} < M_Z < 107 \text{ GeV}$ ,  $E_{e^-} < 90 \text{ GeV}$ ,  $E_{e^+} < 90 \text{ GeV}$ ,  $\cos \theta_{\tau^+\tau^-} < -0.5$ , and  $118 \text{ GeV} < M_{\text{recoil}} < 143 \text{ GeV}$ . The histograms of all cut variables are shown in Figures 29 - 36 (page 13 - 14). Table 2 shows the cut statistics of this mode. For the  $Z \rightarrow \mu^+\mu^-$  mode case, 131.2 signal events and 91.2 background events were remained. The significance was  $S/\sqrt{S+B} = 131.2/\sqrt{131.2+91.2} = 8.8\sigma$ .

Table 1: The cut statistics of  $Z \rightarrow e^+e^-$  mode.

	$eeH$ $H \rightarrow \tau\tau$	$\mu\mu H$ $H \rightarrow \tau\tau$	$\tau\tau H$ $H \rightarrow \tau\tau$	$ZH$ with no $\tau$	$ee\tau\tau$	other 4 leptons	other SM bkg	signi.
No cut	228.3	211.1	214.6	7325	$2.388 \times 10^5$	$5.238 \times 10^5$	$1.492 \times 10^{10}$	0.0019
preselection	171.3	0.155	1.532	47.05	$1.338 \times 10^4$	$3.215 \times 10^4$	$1.023 \times 10^7$	0.053
# of tracks	169.4	0.155	1.532	41.56	$1.316 \times 10^4$	$3.205 \times 10^4$	$1.009 \times 10^7$	0.053
$E_{\text{vis}}$	162.3	0.155	0.912	38.36	$1.068 \times 10^4$	$1.039 \times 10^4$	$4.761 \times 10^6$	0.074
$\cos \theta_{\text{miss}}$	160.6	0.155	0.912	38.03	8719	1906	$5.155 \times 10^5$	0.22
$M_Z$	148.0	0	0.017	29.09	2408	501.2	$1.299 \times 10^4$	1.2
$\cos \theta_{e^-(e^+)}$	133.9	0	0.009	25.40	1067	101.5	729.7	3.0
$E_{e^-(e^+)}$	133.0	0	0.009	24.93	690.3	78.70	629.7	3.4
$\cos \theta_{\tau^+\tau^-}$	130.8	0	0	3.536	254.9	30.70	155.4	5.5
$\cos \theta_{\tau^-(\tau^+)}$	123.4	0	0	3.074	212.1	9.161	3.817	6.6
$M_{\text{recoil}}$	108.9	0	0	2.474	72.35	1.134	0.034	8.0

Table 2: The cut statistics of  $Z \rightarrow \mu^+\mu^-$  mode.

	$\mu\mu H$ $H \rightarrow \tau\tau$	$eeH$ $H \rightarrow \tau\tau$	$\tau\tau H$ $H \rightarrow \tau\tau$	$ZH$ with no $\tau$	$\mu\mu\tau\tau$	other 4 leptons	other SM bkg	signi.
No cut	211.1	228.3	214.6	7325	3513	$7.591 \times 10^6$	$1.492 \times 10^{10}$	0.0017
preselection	168.5	0	0.155	43.01	1698	7546	7732	1.3
# of tracks	167.4	0	0.155	39.65	1684	7537	7400	1.3
$E_{\text{vis}}$	162.9	0	0.155	37.40	1586	2285	3713	1.9
$\cos \theta_{\text{miss}}$	158.6	0	0.155	36.51	1386	227.5	55.48	3.7
$M_Z$	153.2	0	0	32.84	1038	55.28	42.54	4.2
$E_{e^-(e^+)}$	153.2	0	0	32.70	738.6	42.41	36.72	4.8
$\cos \theta_{\tau^+\tau^-}$	146.3	0	0	3.638	259.4	20.19	0.756	7.1
$M_{\text{recoil}}$	131.2	0	0	2.875	82.36	5.311	0.301	8.8

## 4.2 $Z \rightarrow q\bar{q}$ mode

In this mode, the tau pairs are reconstructed first, followed by the di-jet reconstruction of the  $Z$  decay.

At first in this mode, we applied the tau finder to all objects to reconstruct tau leptons. In this analysis, we search the highest energy track and combine the neighboring particles, which satisfy  $\cos \theta_{\text{cone}} > 0.98$ , with the combined mass less than 2 GeV. We regarded the combined object as a tau candidate. Then we applied the selection cuts as following:  $E_{\text{tau candidate}} > 3$  GeV,  $E_{\text{cone}} < 0.1E_{\text{tau candidate}}$  with  $\cos \theta_{\text{cone}} = 0.9$ , and rejecting 3-prong with neutral particles events. These selection cuts were tuned for minimizing misidentification of part of quark jets as tau jets. The survived tau candidate regarded as a tau jet. After the selection cuts, we applied the charge recovery to obtain better efficiency. The charged particles in tau jet which have the energy less than 2 GeV are detached one by one from smallest energy from the tau jet until satisfying the conditions as following: the charge of tau jet is  $+1$  or  $-1$ , and the number of track(s) in tau jet is 1 or 3. The tau jet after detaching is rejected if it does not satisfy the above conditions. After the selection cuts and detaching, we repeat the above processes until there are no charged particles which have the energy greater than 2 GeV.

After the tau reconstruction, we applied the collinear approximation [10] to reconstruct  $M_{\tau^+\tau^-}$ . In this approximation, we assumed that the visible decay products of tau and the neutrino(s) from tau is collinear, and the contribution of missing transverse momentum is only comes from the neutrino(s) of tau decay. The invariant mass of the tau pair with the collinear approximation shown in Figure 16.

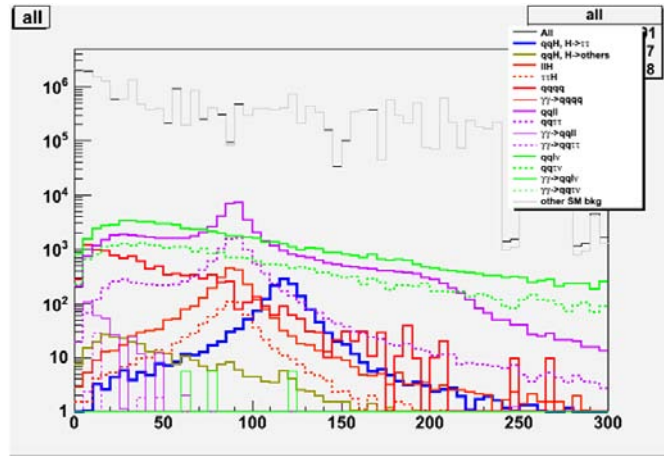


Figure 16: The plot of  $M_{\text{colapp}}$  in the unit of GeV, the invariant mass of di-tau with collinear approximation. Blue histogram shows the signal process  $ZH \rightarrow q\bar{q}\tau\tau$ .

After that, we applied the Durham jet clustering method [11] with two jets for the remaining objects for the reconstruction of the  $Z$  boson.

After the tau and  $Z$  reconstruction, we applied the cuts to select signal process. Before optimizing cuts, we applied the preselection as follows: number of quark jets = 2, number of  $\tau^+$  and  $\tau^- = 1$ , number of tracks in  $\tau \leq 3$ , and the events which have the tracks in both  $\tau = 3$  were rejected (double 3-prong cut). We applied the following cuts to reject the background:  $9 \leq \text{number of tracks} < 50$ ,  $110 \text{ GeV} < E_{\text{vis}} < 235 \text{ GeV}$ ,  $|\cos \theta_{\text{miss}}| < 0.98$ ,  $77 \text{ GeV} < M_Z < 135 \text{ GeV}$ ,  $80 \text{ GeV} < E_Z < 135 \text{ GeV}$ ,  $\cos \theta_{\tau^+\tau^-} < -0.5$ ,  $\log_{10} |d_0/\sigma(d_0)|(\tau^+) + \log_{10} |d_0/\sigma(d_0)|(\tau^-) > -0.7$ ,  $\log_{10} |z_0/\sigma(z_0)|(\tau^+) + \log_{10} |z_0/\sigma(z_0)|(\tau^-) > -0.1$ ,  $M_{\tau^+\tau^-} < 115 \text{ GeV}$ ,  $E_{\tau^+\tau^-} < 125 \text{ GeV}$ ,  $100 \text{ GeV} < M_{\text{colapp}} < 170 \text{ GeV}$ ,  $100 \text{ GeV} < E_{\text{colapp}} < 280 \text{ GeV}$ , and  $112 \text{ GeV} < M_{\text{recoil}} < 160 \text{ GeV}$ , where  $M_{\tau^+\tau^-}$  and  $E_{\tau^+\tau^-}$  is the invariant mass and energy without using collinear approximation,  $M_{\text{colapp}}$  and  $E_{\text{colapp}}$  is the invariant mass and energy with collinear approximation, respec-

tively. The histograms of all cut variables are shown in Figures 37 - 49 (page 14 - 16). Table 3 shows the cut statistics of this mode. After the cuts, the signal events and background events were remained 1026 and 554.4. The statistical significance of  $Z \rightarrow q\bar{q}$  mode is calculated to be  $S/\sqrt{S+B} = 1026/\sqrt{1026+554.4} = 25.8\sigma$ .

Table 3: The cut statistics of  $Z \rightarrow q\bar{q}$  mode.

	$qgH$ $H \rightarrow \tau\tau$	$ZH$ with no $\tau$	$lH$	$\tau\tau H$	$qqqq$	$qql\bar{l}$	$qq\tau\tau$	$qq\ell\nu$	$qq\tau\nu$	other SM bkg	signi.
No cut	4233	$4.829 \times 10^4$	5377	2596	$4.038 \times 10^6$	$3.563 \times 10^5$	$4.169 \times 10^4$	$2.788 \times 10^6$	$1.326 \times 10^6$	$1.494 \times 10^{10}$	0.035
preselection	1647	578.8	2761	765.4	$1.230 \times 10^4$	$6.378 \times 10^4$	$1.161 \times 10^4$	$1.249 \times 10^5$	$4.948 \times 10^4$	$2.570 \times 10^7$	0.32
# of tracks	1644	549.8	2680	765.4	$1.230 \times 10^4$	$6.059 \times 10^4$	$1.146 \times 10^4$	$1.214 \times 10^5$	$4.806 \times 10^4$	$5.190 \times 10^5$	1.9
$E_{\text{vis}}$	1607	492.3	1015	744.2	4443	$2.106 \times 10^4$	$1.107 \times 10^4$	$1.192 \times 10^5$	$4.693 \times 10^4$	$2.383 \times 10^5$	2.4
$\cos \theta_{\text{miss}}$	1572	474.7	860.5	725.1	2127	8315	$1.021 \times 10^4$	$1.171 \times 10^5$	$4.415 \times 10^4$	5939	3.6
$M_Z$	1440	376.1	791.3	682.8	778.6	4987	8674	8189	3288	997.3	8.3
$E_Z$	1429	352.0	782.7	528.7	505.0	4797	7857	7703	3061	609.9	8.6
$\cos \theta_{\tau^+ \tau^-}$	1386	46.28	442.2	255.6	191.4	1468	2001	2831	1154	475.6	13.7
$d_0\text{sig}$	1338	30.29	235.1	244.3	131.4	854.9	1928	1786	1044	248.1	15.1
$z_0\text{sig}$	1287	19.54	105.0	234.7	81.77	408.2	1845	909.9	883.4	244.6	16.6
$M_{\tau^+ \tau^-}$	1286	19.39	103.2	234.7	72.05	349.1	1837	883.5	883.4	243.9	16.7
$E_{\tau^+ \tau^-}$	1282	19.39	103.0	234.7	72.05	324.7	1836	873.2	883.4	243.9	16.7
$M_{\text{colapp}}$	1065	3.074	18.76	47.94	10.28	72.83	616.9	150.8	137.0	0.746	23.1
$E_{\text{colapp}}$	1062	2.454	18.01	46.72	10.28	71.27	612.1	93.05	93.52	0.454	23.7
$M_{\text{recoil}}$	1026	2.144	14.54	21.24	9.938	57.07	366.3	39.64	43.31	0.161	25.8

## 5 Summary

We evaluated the measurement accuracy of the branching ratio of the  $H \rightarrow \tau^+ \tau^-$  mode at  $\sqrt{s} = 250$  GeV at the ILC with ILD\_00 detector model. We assumed  $M_H = 120$  GeV,  $\text{Br}(H \rightarrow \tau^+ \tau^-) = 8.0\%$ ,  $\int L dt = 250 \text{ fb}^{-1}$ , and the polarization  $P(e^+, e^-) = (+0.3, -0.8)$ . The obtained values were summarized in Table 4.

Table 4: The analysis results of  $\sqrt{s} = 250$  GeV.

mode	$Z \rightarrow e^+ e^-$	$Z \rightarrow \mu^+ \mu^-$	$Z \rightarrow q\bar{q}$
significance	$8.0\sigma$	$8.8\sigma$	$25.8\sigma$

From these results, the combined significance was calculated to be  $\sqrt{8.0^2 + 8.8^2 + 25.8^2} = 28.4\sigma$ . Therefore, the measurement accuracy  $\Delta(\sigma \cdot \text{Br})/(\sigma \cdot \text{Br})$  was calculated to be  $\Delta(\sigma \cdot \text{Br})/(\sigma \cdot \text{Br}) = 1/28.4 = 3.5\%$ .

The results are extrapolated to the case of  $M_H = 125$  GeV by scaling the signal yields by the  $e^+ e^- \rightarrow ZH$  cross section and the branching ratio  $\text{Br}(H \rightarrow \tau^+ \tau^-) \rightarrow 6.32\%$  [9]. We assumed that the selection efficiencies the same. The results are summarized in Table 5.

Table 5: The results of the extrapolation to  $M_H = 125$  GeV.

$Z \rightarrow e^+ e^-$	$Z \rightarrow \mu^+ \mu^-$	$Z \rightarrow q\bar{q}$	Combined	$\frac{\Delta(\sigma \cdot \text{Br})}{\sigma \cdot \text{Br}}$
$6.8\sigma$	$7.4\sigma$	$21.9\sigma$	$24.1\sigma$	4.2 %

# A Monte-Carlo Samples

Table 6: Monte-Carlo information which used in this analysis. From the left line, the process ID, process, beam polarization (ep for positrons, em for electrons), cross section in the unit of fb, number of Monte-Carlo events, integrated luminosity in the unit of  $\text{fb}^{-1}$ , are shown. This list continues to Table 7.

21564 aa_bb ep+0,0em+0,0 950,971 95 0,099899	23584 aa_e3e3dd ep+0,0em+0,0 0,073276 10 136,47	21664 ae1_e1e1e1 ep-1,0em+0,0 7275,46 7275 0,999937
21565 aa_bb ep+0,0em+0,0 5218,47 521 0,0998377	23585 aa_e3e3dd ep+0,0em+0,0 0,096953 10 103,143	21665 ae1_e1e1e1 ep-1,0em+0,0 44860,5 44060 0,982156
21566 aa_bb ep+0,0em+0,0 5205,84 520 0,0998878	23586 aa_e3e3dd ep+0,0em+0,0 0,097376 10 102,636	21666 ae1_e1e1e1 ep+1,0em+0,0 7327,35 7327 0,999952
21567 aa_bb ep+0,0em+0,0 4768,41 476 0,0998236	23587 aa_e3e2dd ep+0,0em+0,0 0,019565 10 511,117	21667 ae1_e1e1e1 ep+1,0em+0,0 44910,9 44910 0,99998
21568 aa_cc ep+0,0em+0,0 25826,9 2582 0,0999733	23589 aa_e3e2e3 ep+0,0em+0,0 2,98239 10 3,35302	21668 ae1_e1e2e2 ep+1,0em+0,0 7895,36 7895 0,999954
21569 aa_cc ep+0,0em+0,0 158497 15848 0,0999966	23591 aa_e3e3e3 ep+0,0em+0,0 5,01718 10 1,71905	21669 ae1_e1e2e2 ep+1,0em+0,0 53497,7 52297 0,977556
21570 aa_cc ep+0,0em+0,0 158287 15828 0,0999966	23592 aa_e3e3e3 ep+0,0em+0,0 5,83263 10 1,71449	21670 ae1_e1e2e2 ep+1,0em+0,0 7874,12 6874 0,872996
21571 aa_cc ep+0,0em+0,0 208135 20813 0,0999976	23593 aa_e3e3e3 ep+0,0em+0,0 2,07476 10 4,82137	21671 ae1_e1e2e2 ep+1,0em+0,0 53698,4 52956 0,981369
21572 aa_ccbb ep+0,0em+0,0 0,01058 10 347,329	23594 aa_e3e3ss ep+0,0em+0,0 0,07357 10 136,32	21672 ae1_e1e3e3 ep+1,0em+0,0 13442,9 13442 0,999933
21573 aa_ccbb ep+0,0em+0,0 0,004464 10 2240,14	23595 aa_e3e3ss ep+0,0em+0,0 0,09712 10 102,365	21673 ae1_e1e3e3 ep+1,0em+0,0 96101,5 94701 0,986427
21574 aa_ccbb ep+0,0em+0,0 0,004558 10 2205,61	23596 aa_e3e3ss ep+0,0em+0,0 0,097381 10 102,689	21674 ae1_e1e3e3 ep+1,0em+0,0 13483 13283 0,986167
21575 aa_ccccc ep+0,0em+0,0 0,038923 10 256,918	23597 aa_e3e3ss ep+0,0em+0,0 0,019563 10 509,217	21675 ae1_e1e3e3 ep+1,0em+0,0 96257,6 94057 0,977138
21576 aa_ccccc ep+0,0em+0,0 0,012718 10 786,287	23598 aa_niel1du ep+0,0em+0,0 0,225273 10 44,3906	21676 ae1_e1n2h2 ep+1,0em+0,0 33,3463 33 0,986915
21577 aa_ccccc ep+0,0em+0,0 0,010308 10 764,526	23599 aa_niel1el1 ep+0,0em+0,0 0,076331 10 130,998	21677 ae1_e1n2h2 ep+1,0em+0,0 14,4871 14 0,966377
21578 aa_cccd ep+0,0em+0,0 0,008955 10 1116,69	23600 aa_niel1el1 ep+0,0em+0,0 0,073443 10 136,16	21678 ae1_e1n2h2 ep+1,0em+0,0 52,0695 52 0,998665
21579 aa_cccd ep+0,0em+0,0 0,002019 10 4912,95	23601 aa_niel1el3 ep+0,0em+0,0 0,073751 10 135,58	21679 ae1_e1n2h2 ep+1,0em+0,0 22,6358 22 0,971912
21580 aa_cccd ep+0,0em+0,0 0,002071 10 4828,59	23602 aa_niel1el3 ep+0,0em+0,0 0,07357 10 136,32	21680 ae1_e1n3h3 ep+1,0em+0,0 33,3835 33 0,988509
21581 aa_cccd ep+0,0em+0,0 0,004750 10 21,0525	23603 aa_niel1el3 ep+0,0em+0,0 0,07357 10 136,32	21681 ae1_e1n3h3 ep+1,0em+0,0 14,5035 14 0,965284
21582 aa_cccd ep+0,0em+0,0 0,005743 10 17,4144	23604 aa_niel1el3 ep+0,0em+0,0 0,07357 10 136,32	21682 ae1_e1n3h3 ep+1,0em+0,0 52,1148 52 0,997797
21583 aa_cccd ep+0,0em+0,0 0,005743 10 17,299	23605 aa_niel1el3 ep+0,0em+0,0 0,07357 10 136,32	21683 ae1_e1n3h3 ep+1,0em+0,0 22,6013 22 0,973395
21584 aa_cccd ep+0,0em+0,0 0,095692 10 104,186	23606 aa_niel1el3 ep+0,0em+0,0 0,07357 10 136,32	21684 ae1_e1n2h2 ep+1,0em+0,0 265,497 263 0,998114
21585 aa_cccd ep+0,0em+0,0 0,073937 10 21,0999	23607 aa_niel1el3 ep+0,0em+0,0 0,07357 10 136,32	21685 ae1_e1n2h2 ep+1,0em+0,0 1205,28 1200 0,999768
21586 aa_cccd ep+0,0em+0,0 0,073748 10 17,2787	23608 aa_niel1el3 ep+0,0em+0,0 0,07357 10 136,32	21686 ae1_e1n2h2 ep+1,0em+0,0 1203,83 1203 0,999311
21587 aa_cccd ep+0,0em+0,0 0,058165 10 17,1926	23609 aa_niel1el3 ep+0,0em+0,0 0,07357 10 136,32	21687 ae1_e1n2h2 ep+1,0em+0,0 2630,42 2630 0,99984
21588 aa_cccd ep+0,0em+0,0 0,005940 10 104,817	23610 aa_niel1el3 ep+0,0em+0,0 0,07357 10 136,32	21688 ae1_e1n2h2 ep+1,0em+0,0 14,4117,2 14117 0,999986
21589 aa_cccd ep+0,0em+0,0 0,022543 10 12,356	23611 aa_niel1el3 ep+0,0em+0,0 0,07357 10 136,32	21689 ae1_e1n2h2 ep+1,0em+0,0 14,4189,1 14189 0,999993
21590 aa_cccd ep+0,0em+0,0 1,07006 10 9,34527	23612 aa_niel1el3 ep+0,0em+0,0 0,07357 10 136,32	21690 bb ep+1,0em+1,0 47506,1 99600 2,09567
21591 aa_cccd ep+0,0em+0,0 0,095692 10 50,3497	23613 aa_niel1el3 ep+0,0em+0,0 0,07357 10 136,32	21691 bb ep+1,0em+1,0 27565 99800 3,6204
21592 aa_cccd ep+0,0em+0,0 0,198611 10 50,3497	23614 aa_niel1el3 ep+0,0em+0,0 0,07357 10 136,32	21692 bbbb ep+1,0em+1,0 67,0078 67009 1000
21593 aa_cccd ep+0,0em+0,0 0,644154 10 15,524	23615 aa_niel1el3 ep+0,0em+0,0 0,07357 10 136,32	21693 bbbb ep+1,0em+1,0 28,7721 28772 999,997
21594 aa_cccd ep+0,0em+0,0 0,001171 10 8539,71	23616 aa_niel1el3 ep+0,0em+0,0 0,07357 10 136,32	21694 bbcsdu ep+1,0em+1,0 0,029070 10000 334270
21595 aa_cccd ep+0,0em+0,0 0,002159 10 44,4071	23617 aa_niel1el3 ep+0,0em+0,0 0,07357 10 136,32	21695 bbccss ep+1,0em+1,0 0,034435 10000 290402
21596 aa_cccd ep+0,0em+0,0 0,0225196 10 44,4058	23618 aa_niel1el3 ep+0,0em+0,0 0,07357 10 136,32	21696 bbccss ep+1,0em+1,0 0,002779 10000 3,59842e+06
21597 aa_cccd ep+0,0em+0,0 0,0225458 10 44,3522	23619 aa_niel1el3 ep+0,0em+0,0 0,07357 10 136,32	21697 bbccss ep+1,0em+1,0 0,002779 10000 2,235901
21598 aa_cccd ep+0,0em+0,0 0,002852 10 3506,31	23620 aa_niel1el3 ep+0,0em+0,0 0,07357 10 136,32	21698 bbccss ep+1,0em+1,0 75,502 7502 1,000
21599 aa_cccd ep+0,0em+0,0 0,003221 10 3104,63	23621 aa_niel1el3 ep+0,0em+0,0 0,07357 10 136,32	21699 bbccss ep+1,0em+1,0 48,4438 48444 1000
21600 aa_dd ep+0,0em+0,0 1611,35 161 0,0939162	23622 aa_niel1el3 ep+0,0em+0,0 0,07357 10 136,32	22000 bbdudu ep+1,0em+1,0 0,033996 10000 294239
21601 aa_dd ep+0,0em+0,0 9902,35 990 0,0939363	23623 aa_niel1el3 ep+0,0em+0,0 0,07357 10 136,32	22001 bbdudu ep+1,0em+1,0 0,002776 10000 3,60231e+06
21602 aa_dd ep+0,0em+0,0 0,0935672 10 3935672	23624 aa_niel1el3 ep+0,0em+0,0 0,07357 10 136,32	22002 bbdudu ep+1,0em+1,0 0,030041 10000 332287
21603 aa_dd ep+0,0em+0,0 9913,28 991 0,0935672	23625 aa_niel1el3 ep+0,0em+0,0 0,07357 10 136,32	22003 bbdudu ep+1,0em+1,0 44745,7 99000 2,23591
21604 aa_dd ep+0,0em+0,0 12995,6 1299 0,0939723	23626 aa_niel1el3 ep+0,0em+0,0 0,07357 10 136,32	22004 bbdudu ep+1,0em+1,0 27317,2 88000 3,24338
21605 aa_e1el ep+0,0em+0,0 794745,4 7947 0,099928	23627 aa_niel1el3 ep+0,0em+0,0 0,07357 10 136,32	22005 bbdudu ep+1,0em+1,0 123,789 99000 799,748
21606 aa_e1el ep+0,0em+0,0 551033 10 107786,1 0,196507	23628 aa_niel1el3 ep+0,0em+0,0 0,07357 10 136,32	22006 bbdudu ep+1,0em+1,0 56,6712 55671 982,381
21607 aa_e1el ep+0,0em+0,0 1,424316 10 137431 0,0964895	23629 aa_niel1el3 ep+0,0em+0,0 0,07357 10 136,32	22007 bbdudu ep+1,0em+1,0 54,3738 5374 988,974
21608 aa_e1elbb ep+0,0em+0,0 0,031025 10 322,321	23630 aa_niel1el3 ep+0,0em+0,0 0,07357 10 136,32	22008 bbdudu ep+1,0em+1,0 26,3297 26330 1000,01
21609 aa_e1elbb ep+0,0em+0,0 0,028705 10 348,371	23631 aa_niel1el3 ep+0,0em+0,0 0,07357 10 136,32	22009 bbdudu ep+1,0em+1,0 0,003422 10000 2,92227e+06
21610 aa_e1elbb ep+0,0em+0,0 0,002884 10 346,741	23632 aa_niel1el3 ep+0,0em+0,0 0,07357 10 136,32	22010 bbdudu ep+1,0em+1,0 37,8798 37900 1000,01
21611 aa_e1elbb ep+0,0em+0,0 0,002885 10 346,741	23633 aa_niel1el3 ep+0,0em+0,0 0,07357 10 136,32	22011 bbdudu ep+1,0em+1,0 55,1354 52335 996,229
21612 aa_e1elbb ep+0,0em+0,0 0,002885 10 346,741	23634 aa_niel1el3 ep+0,0em+0,0 0,07357 10 136,32	22012 bbdudu ep+1,0em+1,0 56,5712 55671 982,381
21613 aa_e1elbb ep+0,0em+0,0 0,002885 10 346,741	23635 aa_niel1el3 ep+0,0em+0,0 0,07357 10 136,32	22013 bbdudu ep+1,0em+1,0 54,3738 5374 988,974
21614 aa_e1elbb ep+0,0em+0,0 0,002885 10 346,741	23636 aa_niel1el3 ep+0,0em+0,0 0,07357 10 136,32	22014 bbdudu ep+1,0em+1,0 29,1511 29151 993,997
21615 aa_e1elbb ep+0,0em+0,0 0,002885 10 346,741	23637 aa_niel1el3 ep+0,0em+0,0 0,07357 10 136,32	22015 bbdudu ep+1,0em+1,0 59,231 59231 1000,01
21616 aa_e1elbb ep+0,0em+0,0 0,002885 10 346,741	23638 aa_niel1el3 ep+0,0em+0,0 0,07357 10 136,32	22016 bbdudu ep+1,0em+1,0 37,8798 37900 1000,01
21617 aa_e1elbb ep+0,0em+0,0 0,002885 10 346,741	23639 aa_niel1el3 ep+0,0em+0,0 0,07357 10 136,32	22017 bbdudu ep+1,0em+1,0 55,1354 52335 996,229
21618 aa_e1elbb ep+0,0em+0,0 0,002885 10 346,741	23640 aa_niel1el3 ep+0,0em+0,0 0,07357 10 136,32	22018 bbdudu ep+1,0em+1,0 55,1354 52335 996,229
21619 aa_e1elbb ep+0,0em+0,0 0,002885 10 346,741	23641 aa_niel1el3 ep+0,0em+0,0 0,07357 10 136,32	22019 bbdudu ep+1,0em+1,0 55,1354 52335 996,229
21620 aa_e1elbb ep+0,0em+0,0 0,002885 10 346,741	23642 aa_niel1el3 ep+0,0em+0,0 0,07357 10 136,32	22020 bbdudu ep+1,0em+1,0 55,1354 52335 996,229
21621 aa_e1elbb ep+0,0em+0,0 0,002885 10 346,741	23643 aa_niel1el3 ep+0,0em+0,0 0,07357 10 136,32	22021 bbdudu ep+1,0em+1,0 55,1354 52335 996,229
21622 aa_e1elbb ep+0,0em+0,0 0,002885 10 346,741	23644 aa_niel1el3 ep+0,0em+0,0 0,07357 10 136,32	22022 bbdudu ep+1,0em+1,0 55,1354 52335 996,229
21623 aa_e1elbb ep+0,0em+0,0 0,002885 10 346,741	23645 aa_niel1el3 ep+0,0em+0,0 0,07357 10 136,32	22023 bbdudu ep+1,0em+1,0 55,1354 52335 996,229
21624 aa_e1elbb ep+0,0em+0,0 0,002885 10 346,741	23646 aa_niel1el3 ep+0,0em+0,0 0,07357 10 136,32	22024 bbdudu ep+1,0em+1,0 55,1354 52335 996,229
21625 aa_e1elbb ep+0,0em+0,0 0,002885 10 346,741	23647 aa_niel1el3 ep+0,0em+0,0 0,07357 10 136,32	22025 bbdudu ep+1,0em+1,0 55,1354 52335 996,229
21626 aa_e1elbb ep+0,0em+0,0 0,002885 10 346,741	23648 aa_niel1el3 ep+0,0em+0,0 0,07357 10 136,32	22026 bbdudu ep+1,0em+1,0 55,1354 52335 996,229
21627 aa_e1elbb ep+0,0em+0,0 0,002885 10 346,741	23649 aa_niel1el3 ep+0,0em+0,0 0,07357 10 136,32	22027 bbdudu ep+1,0em+1,0 55,1354 52335 996,229
21628 aa_e1elbb ep+0,0em+0,0 0,002885 10 346,741	23650 aa_niel1el3 ep+0,0em+0,0 0,07357 10 136,32	22028 bbdudu ep+1,0em+1,0 55,1354 52335 996,229
21629 aa_e1elbb ep+0,0em+0,0 0,002885 10 346,741	23651 aa_niel1el3 ep+0,0em+0,0 0,07357 10 136,32	22029 bbdudu ep+1,0em+1,0 55,1354 52335 996,229
21630 aa_e1elbb ep+0,0em+0,0 0,002885 10 346,741	23652 aa_niel1el3 ep+0,0em+0,0 0,07357 10 136,32	22030 bbdudu ep+1,0em+1,0 55,1354 52335 996,229
21631 aa_e1elbb ep+0,0em+0,0 0,002885 10 346,741	23653 aa_niel1el3 ep+0,0em+0,0 0,07357 10 136,32	22031 bbdudu ep+1,0em+1,0 55,1354 52335 996,229
21632 aa_e1elbb ep+0,0em+0,0 0,002885 10 346,741	23654 aa_niel1el3 ep+0,0em+0,0 0,07357 10 136,32	22032 bbdudu ep+1,0em+1,0 55,1354 52335 996,229
21633 aa_e1elbb ep+0,0em+0,0 0,002885 10 346,741	23655 aa_niel1el3 ep+0,0em+0,0 0,07357 10 136,32	22033 bbdudu ep+1,0em+1,0 55,1354 52335 996,229
21634 aa_e1elbb ep+0,0em+0,0 0,002885 10 346,741	23656 aa_niel1el3 ep+0,0em+0,0 0,07357 10 136,32	22034 bbdudu ep+1,0em+1,0 55,1354 52335 996,229
21635 aa_e1elbb ep+0,0em+0,0 0,002885 10 346,741	23657 aa_niel1el3 ep+0,0em+0,0 0,07357 10 136,32	22035 bbdudu ep+1,0em+1,0 55,1354 52335 996,229
21636 aa_e1elbb ep+0,0em+0,0 0,002885 10 346,741	23658 aa_niel1el3 ep+0,0em+0,0 0,07357 10 136,32	22036 bbdudu ep+1,0em+1,0 55,1354 52335 996,229
21637 aa_e1elbb ep+0,0em+0,0 0,002885 10 346,741	23659 aa_niel1el3 ep+0,0em+0,0 0,07357 10 136,32	22037 bbdudu ep+1,0em+1,0 55,1354 52335 996,229
21638 aa_e1elbb ep+0,0em+0,0 0,002885 10 346,741	23660 aa_niel1el3 ep+0,0em+0,0 0,07357 10 136,32	22038 bbdudu ep+1,0em+1,0 55,1354 52335 996,229
21639 aa_e1elbb ep+0,0em+0,0 0,002885 10 346,741	23661 aa_niel1el3 ep+0,0em+0,0 0,07357 10 136,32	22039 bbdudu ep+1,0em+1,0 55,1354 52335 996,229
21640 aa_e1elbb ep+0,0em+0,0 0,002885 10 346,741	23662 aa_niel1el3 ep+0,0em+0,0 0,07357 10 136,32	22

Table 7: Monte-Carlo information which used in this analysis. From the left line, the process ID, process, beam polarization (ep for positrons, em for electrons), cross section in the unit of fb, number of Monte-Carlo events, integrated luminosity in the unit of  $\text{fb}^{-1}$ , are shown. This list is series of Table 6.

21600	e1a_e1cc	ep+0.0em+1.0	2692.03	2000	0.742934	21216	n1e1e1n1	ep-1.0em+1.0	43,5841	43384	995.409	21397	n3n3e2e2	ep+1.0em+1.0	24,7238	24324	983.829	
21601	e1a_e1cc	ep+0.0em+1.0	14258.4	14230.76	0.999972	21217	n1e1e1n1	ep+1.0em+1.0	933,999	98800	105,207	21398	n3n3e2e2	ep-1.0em+1.0	12,8475	12847	999.961	
21602	e1a_e1cc	ep+0.0em+1.0	2630.76	2630	0.999711	21218	n1e1e1n1	ep-1.0em+1.0	27,4575	26858	978.166	20601	n3n3h	ep+1.0em+1.0	33,8138	33814	1000.01	
21603	e1a_e1cc	ep+0.0em+1.0	14172	14172	1	21219	n1e1e1n1	ep+1.0em+1.0	43,6248	43625	1000	20602	n3n3h	ep-1.0em+1.0	21,6936	21694	1000.02	
21616	e1a_e1dd	ep+0.0em+1.0	305,228	305	0.999923	21220	n1e1e2n2	ep+1.0em+1.0	28,824	28424	986.123	21405	n3n3ss	ep+1.0em+1.0	60,567	60567	1000	
21617	e1a_e1dd	ep+0.0em+1.0	1207.73	1207	0.999936	21221	n1e1e2n2	ep+1.0em+1.0	822,5	98000	119,149	21406	n3n3ss	ep-1.0em+1.0	25,5588	25556	1000.01	
21618	e1a_e1dd	ep+0.0em+1.0	253,502	253	0.997716	21222	n1e1e2n2	ep+1.0em+1.0	7,09688	10000	1409,07	21333	n3n3uu	ep+1.0em+1.0	54,5087	54109	982,667	
21619	e1a_e1dd	ep+0.0em+1.0	1210.08	1210	0.999934	21224	n1e1e3n3	ep-1.0em+1.0	28,6769	28477	993.029	21334	n3n3uu	ep-1.0em+1.0	24,5484	24348	991.836	
21604	e1a_e1e1	ep+0.0em+1.0	7311,26	7311	0.999964	21225	n1e1e3n3	ep+1.0em+1.0	823,729	97800	118,728	21185	ss	ep+1.0em+1.0	48249,2	98200	2,03527	
21605	e1a_e1e1	ep+0.0em+1.0	45047.4	43047	0.955587	21226	n1e1e3n3	ep-1.0em+1.0	7,10283	10000	1407,89	21186	ss	ep-1.0em+1.0	28018,8	89400	3,54762	
21606	e1a_e1e1	ep+0.0em+1.0	7282,56	7282	0.999923	21232	n1e1sc	ep-1.0em+1.0	86,1229	86123	1000	21529	ssbb	ep+1.0em+1.0	137,055	100000	729,634	
21607	e1a_e1e1	ep+0.0em+1.0	44999.4	43999	0.977769	21233	n1e1sc	ep+1.0em+1.0	2470,34	10000	40,4803	21530	ssbb	ep-1.0em+1.0	58,9474	58947	999,993	
21608	e1a_e1e2	ep+0.0em+1.0	7,7880	39	7880	0.99995	21234	n1e1sc	ep-1.0em+1.0	20,9005	20701	990,455	20629	ssh	ep+1.0em+1.0	75,8803	75880	999,996
21609	e1a_e1e2	ep+0.0em+1.0	53381,4	53414	0.992559	21225	n1n1a	ep+1.0em+1.0	7,09688	10000	1409,07	20630	ssh	ep-1.0em+1.0	48,5657	48566	1000,01	
21610	e1a_e1e2	ep+0.0em+1.0	7,9869,66	7869	0.999916	21226	n1n1a	ep+1.0em+1.0	2878,85	27788	9,65247	21525	ssss	ep+1.0em+1.0	67,1388	66739	994,045	
21611	e1a_e1e2	ep+0.0em+1.0	53768,5	50565	0.940468	21237	n1n1a	ep+1.0em+1.0	1582,94	15829	9,99975	21526	ssss	ep-1.0em+1.0	28,8318	28832	1000,01	
21612	e1a_e1e3	ep+0.0em+1.0	13,4741,9	13471	0.999933	21238	n1n1aa	ep+1.0em+1.0	281,145	2811	9,9984	24993	ssssbb	ep+1.0em+1.0	0,001091	10000	9,1659e+06	
21613	e1a_e1e3	ep+0.0em+1.0	9,6603,4	94803	0.981363	21239	n1n1aa	ep+1.0em+1.0	63,1909	632	10,0013	21289	udu	ep+1.0em+1.0	6633,45	100000	15,0751	
21614	e1a_e1e3	ep+0.0em+1.0	13,3459,7	13454	0.999948	21240	n1n1aa	ep+1.0em+1.0	16,0647	161	10,022	21290	udu	ep+1.0em+1.0	112,876	99400	880,612	
21615	e1a_e1e3	ep+0.0em+1.0	9,6607,9	95607	0.989649	21241	n1n1bb	ep+1.0em+1.0	85,7148	87515	1000	21277	ude1n1	ep+1.0em+1.0	2467,75	98200	39,7933	
21588	e1a_e1n2	ep+0.0em+1.0	52,02727	52	0.998604	21242	n1n1bb	ep+1.0em+1.0	25,0179	25018	1000	21278	ude1n1	ep+1.0em+1.0	20,8973	20897	999,986	
21589	e1a_e1n2	ep+0.0em+1.0	21,8282	21	0.962058	21243	n1n1c	ep+1.0em+1.0	81,3195	81319	999,994	21279	ude1n1	ep+1.0em+1.0	86,4364	86036	995,368	
21590	e1a_e1n2	ep+0.0em+1.0	33,307	33	0.999783	21244	n1n1c	ep-1.0em+1.0	24,5259	24526	1000	21281	ude2n2	ep+1.0em+1.0	2268,37	89800	39,5879	
21591	e1a_e1n2	ep+0.0em+1.0	13,982	14	0.00129	21245	n1n1d	ep+1.0em+1.0	87,9093	87899	999,997	21282	ude2n2	ep+1.0em+1.0	20,9171	13717	942,626	
21592	e1a_e1n3	ep+0.0em+1.0	52,0479	52	0.999908	21246	n1n1d	ep+1.0em+1.0	25,5486	25545	1000,02	21285	ude3n3	ep+1.0em+1.0	2263,51	100000	44,1792	
21593	e1a_e1n3	ep+0.0em+1.0	21,8319	21	0.961895	21247	n1n1e2	ep+1.0em+1.0	44,7068	42707	955,269	21286	ude3n3	ep+1.0em+1.0	20,8931	20893	999,995	
21594	e1a_e1n3	ep+0.0em+1.0	33,3573	33	0.998289	21248	n1n1e2	ep+1.0em+1.0	12,8466	12847	1000,03	21293	udscc	ep+1.0em+1.0	6522,1	98900	15,1178	
21595	e1a_e1n3	ep+0.0em+1.0	13,9806	14	0.00139	21249	n1n1e3	ep+1.0em+1.0	44,4167	43417	977,433	21294	udscc	ep+1.0em+1.0	59,9897	59130	986,669	
21596	e1a_e1s	ep+0.0em+1.0	305,28	305	0.999083	21250	n1n1e3	ep+1.0em+1.0	12,7892	12789	999,984	21161	uu	ep+1.0em+1.0	44890,2	88900	2,00044	
21597	e1a_e1s	ep+0.0em+1.0	1203,61	1203	0.999493	21251	n1n1h	ep+1.0em+1.0	60,8309	60831	1000	21162	uu	ep+1.0em+1.0	27372	95400	3,49531	
21598	e1a_e1u	ep+0.0em+1.0	2631,22	2631	0.999916	20593	n1n1h	ep+1.0em+1.0	21,6813	19881	999,986	21429	uubb	ep+1.0em+1.0	123,961	99400	801,865	
21599	e1a_e1u	ep+0.0em+1.0	14186,3	14186	0.999979	21252	n1n1iss	ep+1.0em+1.0	87,6368	87637	1000	21430	uubb	ep+1.0em+1.0	56,7304	56330	932,942	
21600	e1a_e1u	ep+0.0em+1.0	1,725424	1,725424	0.00144892	21253	n1n1iss	ep+1.0em+1.0	25,4646	25465	1000,02	21345	uucc	ep+1.0em+1.0	109,296	99200	907,627	
21601	e1a_e1u	ep+0.0em+1.0	1,733747	1,733747	0.00129777	21254	n1n1u	ep+1.0em+1.0	81,2845	81084	997,533	21346	uucc	ep+1.0em+1.0	52,8917	52892	1000,01	
21602	e1a_e1u	ep+0.0em+1.0	1,729464	1,729464	0.00141663	21255	n1n1u	ep+1.0em+1.0	24,5303	24330	991,835	21447	uuccbb	ep+1.0em+1.0	0,006857	10000	1,46263e+06	
21603	e1a_e1u	ep+0.0em+1.0	1,725171	1,725171	0.00144913	21256	n1n2e2d	ep+1.0em+1.0	20,822,26	24,876	116,507	21448	uuccbb	ep+1.0em+1.0	0,003574	10000	2,79795e+06	
21604	e1a_e1u	ep+0.0em+1.0	57,2207	57,2207	1,000,01	21257	n2e2e1n1	ep+1.0em+1.0	12,7892	12789	116,726	21417	uue2e2	ep+1.0em+1.0	53,0187	53019	1000,01	
21605	e1a_e1u	ep+0.0em+1.0	1,725424	1,725424	0.00144892	21258	n2e2e2n1	ep+1.0em+1.0	12,7892	12789	116,507	21418	uue2e2	ep+1.0em+1.0	29,2735	29274	1000,01	
21606	e1a_e1u	ep+0.0em+1.0	1,729464	1,729464	0.00141663	21259	n2e2e3n3	ep+1.0em+1.0	12,755	12,755	128,968	21421	uue3e3	ep+1.0em+1.0	52,7824	52562	996,203	
21607	e1a_e1u	ep+0.0em+1.0	1,725171	1,725171	0.00144913	21260	n2e2e3n3	ep+1.0em+1.0	12,71024	12,9400	132,224	21422	uue3e3	ep+1.0em+1.0	29,0929	27939	958,756	
21608	e1a_e1u	ep+0.0em+1.0	1,725171	1,725171	0.00144913	20605	uuuh	ep+1.0em+1.0	59,1744	59174	999,993	20606	uuuh	ep+1.0em+1.0	37,9259	37926	1000,00	
21609	e1a_e1u	ep+0.0em+1.0	1,725171	1,725171	0.00144913	21261	uuhh	ep+1.0em+1.0	120,889	98800	816,603	21425	uuss	ep+1.0em+1.0	120,889	98800	816,603	
21610	e1a_e1u	ep+0.0em+1.0	1,725171	1,725171	0.00144913	21262	uuhh	ep+1.0em+1.0	55,1501	53395	978,239	24713	uussbb	ep+1.0em+1.0	0,004512	10000	2,21631e+06	
21611	e1a_e1u	ep+0.0em+1.0	1,725171	1,725171	0.00144913	21263	uuhh	ep+1.0em+1.0	28,5789	24579	1000,02	24714	uussbb	ep+1.0em+1.0	0,002273	10000	4,33947e+06	
21612	e1a_e1u	ep+0.0em+1.0	1,725171	1,725171	0.00144913	21264	uuhh	ep+1.0em+1.0	12,7721	11772	112,697	21341	uuu	ep+1.0em+1.0	54,3813	50981	937,473	
21613	e1a_e1u	ep+0.0em+1.0	17,8919	17,892	1,000,01	20597	n2n2h	ep+1.0em+1.0	33,8388	33839	1000,01	21342	uuu	ep+1.0em+1.0	26,5337	26134	992,417	
21614	e1a_e1u	ep+0.0em+1.0	11,2894	11,2894	999,965	20598	n2n2h	ep+1.0em+1.0	21,6474	21647	999,982	24441	uuuubb	ep+1.0em+1.0	0,003435	10000	2,91121e+06	
21615	e1a_e1u	ep+0.0em+1.0	1,645477	1,645477	1,000,01	21265	n2n2h2	ep+1.0em+1.0	20,8481	20248	971,216	24442	uuuubb	ep+1.0em+1.0	0,001759	10000	5,68505e+06	
21616	e1a_e1u	ep+0.0em+1.0	1,645477	1,645477	1,000,01	21266	n2n2h2	ep+1.0em+1.0	12,7721	11772	112,697	21373	n2n2e3	ep+1.0em+1.0	12,7721	11772	112,697	
21617	e1a_e1u	ep+0.0em+1.0	1,645477	1,645477	1,000,01	21267	n2n2e3	ep+1.0em+1.0	12,7721	11772	112,697	21374	n2n2e1e1	ep+1.0em+1.0	12,7721	11772	112,697	
21618	e1a_e1u	ep+0.0em+1.0	1,645477															

## B Histograms of cut variables

### B.1 $Z \rightarrow e^+e^-$ mode

Figures 17 - 28 show the histograms of cut variables. The blue lines in all histograms show the signal process  $ZH \rightarrow e^+e^-\tau^+\tau^-$ .

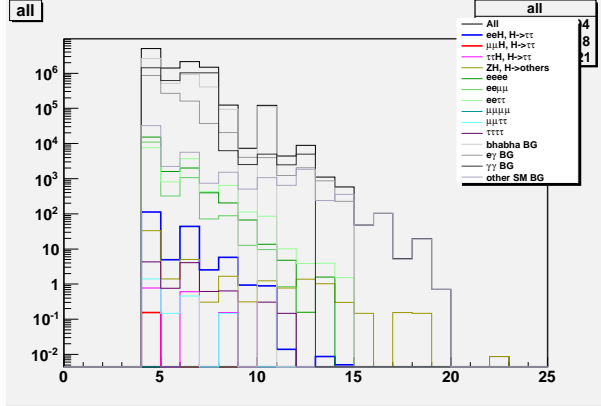


Figure 17: Number of tracks  $\leq 8$ .

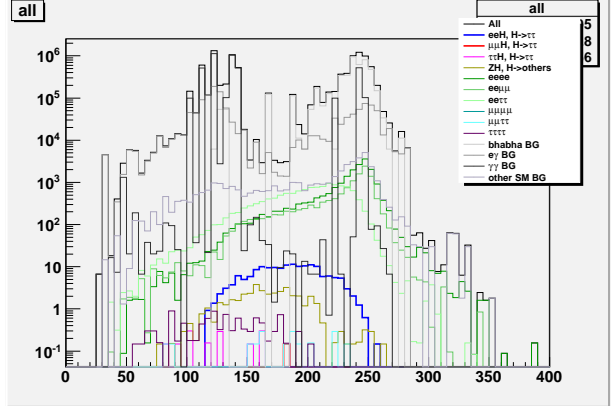


Figure 18:  $115 \text{ GeV} < E_{\text{vis}} < 230 \text{ GeV}$ .

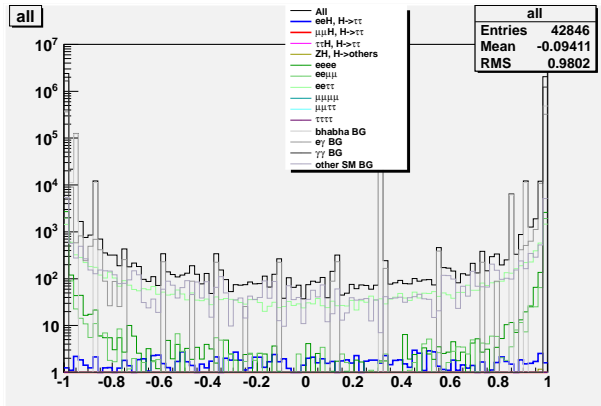


Figure 19:  $|\cos \theta_{\text{miss}}| < 0.99$ .

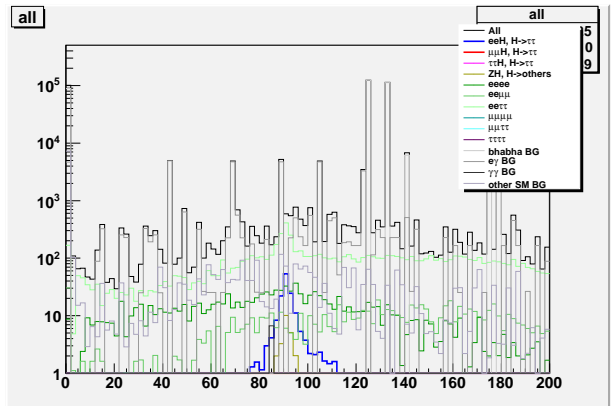


Figure 20:  $81 \text{ GeV} < M_Z < 113 \text{ GeV}$ .

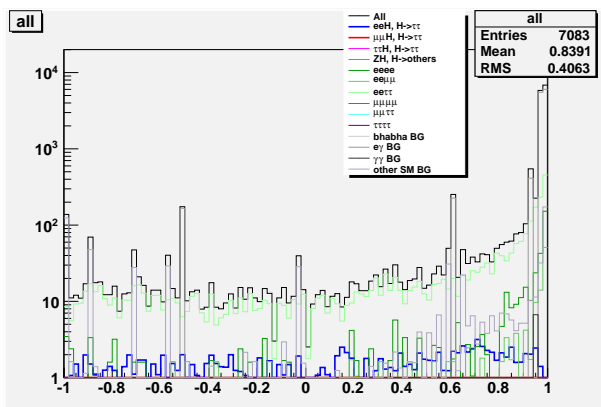


Figure 21:  $\cos \theta_{e^-} < 0.92$ .

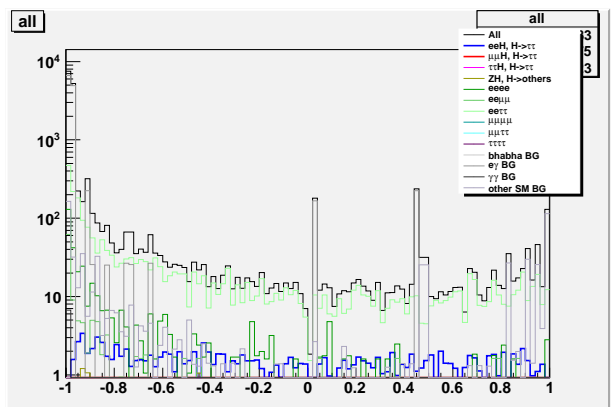


Figure 22:  $\cos \theta_{e^+} > -0.92$ .

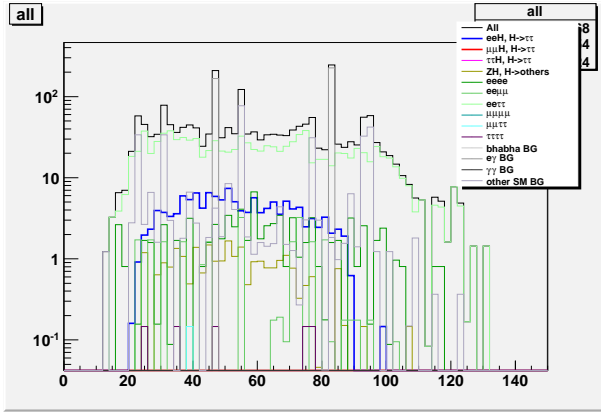


Figure 23:  $E_{e^-} < 90$  GeV.

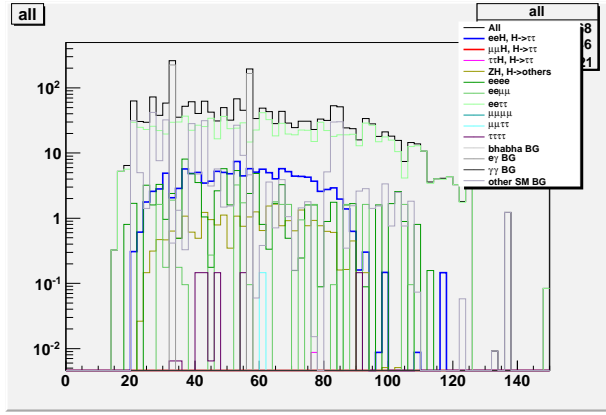


Figure 24:  $E_{e^+} < 90$  GeV.

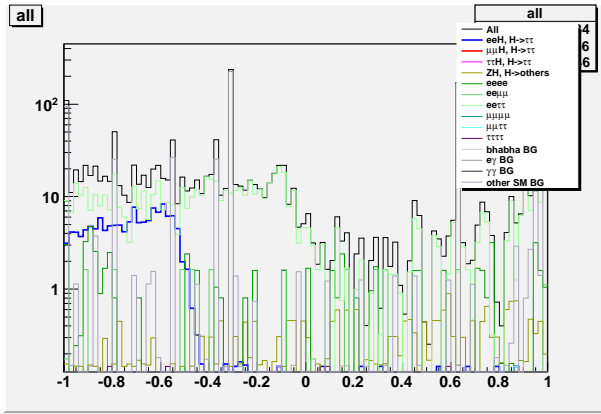


Figure 25:  $\cos \theta_{\tau^+\tau^-} < -0.45$ .

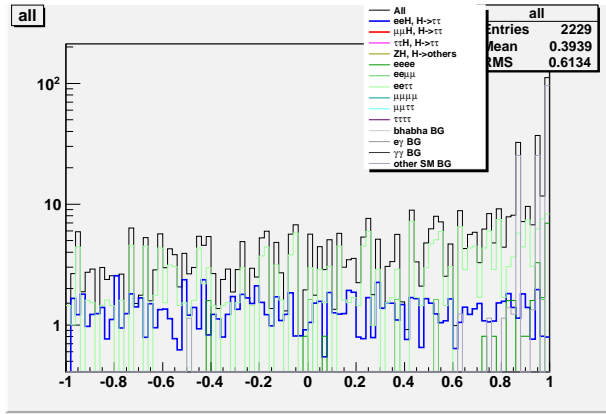


Figure 26:  $\cos \theta_{\tau^-} < 0.92$ .

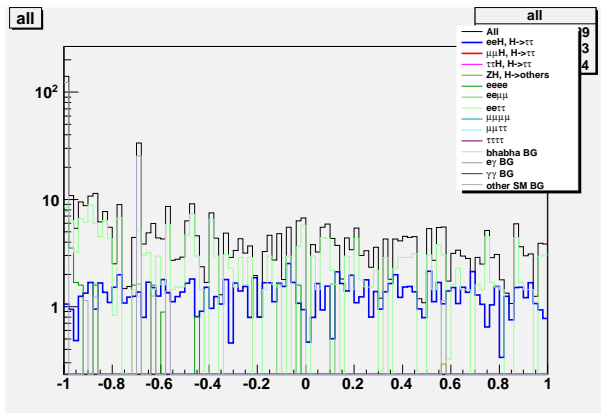


Figure 27:  $\cos \theta_{\tau^+} > -0.92$ .

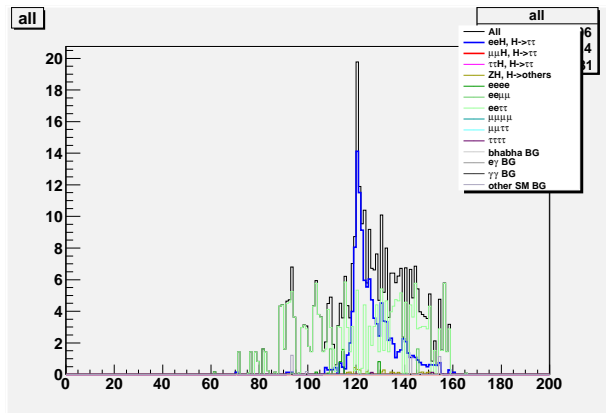
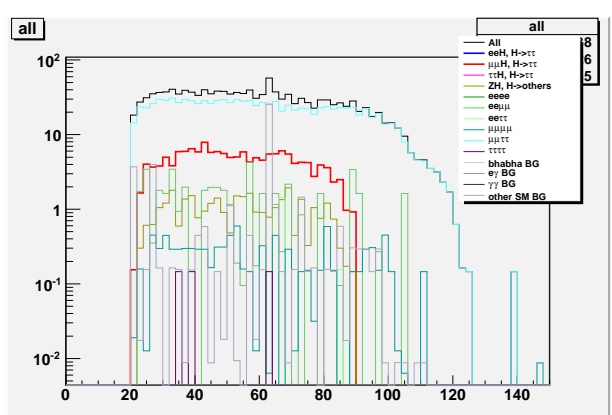
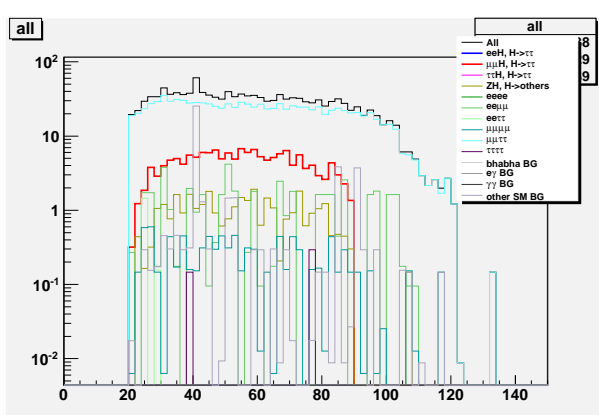
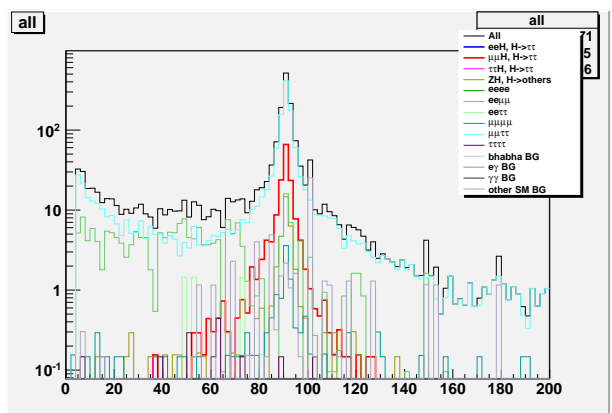
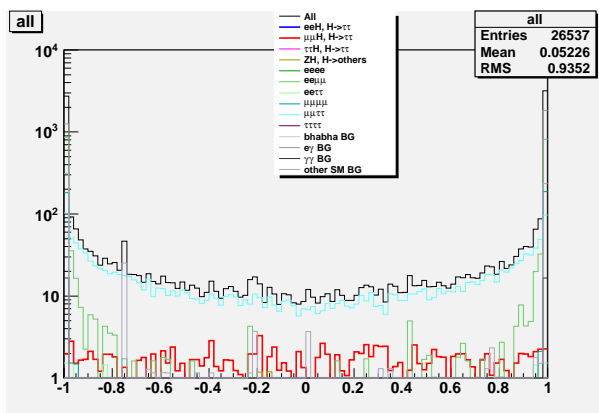
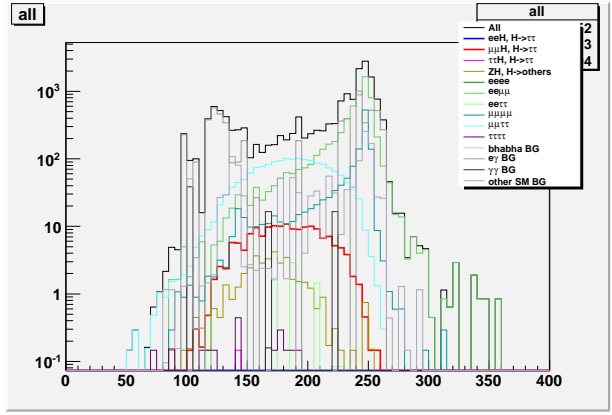
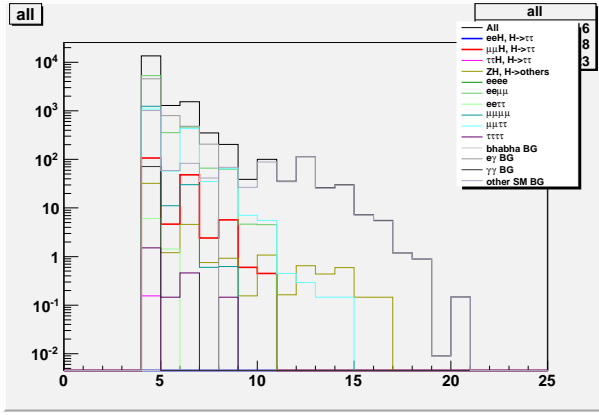


Figure 28:  $116 \text{ GeV} < M_{\text{recoil}} < 142 \text{ GeV}$ .

## B.2 $Z \rightarrow \mu^+ \mu^-$ mode

Figures 29 - 36 show the histograms of cut variables. The red lines in all histograms show the signal process  $ZH \rightarrow \mu^+ \mu^- \tau^+ \tau^-$ .



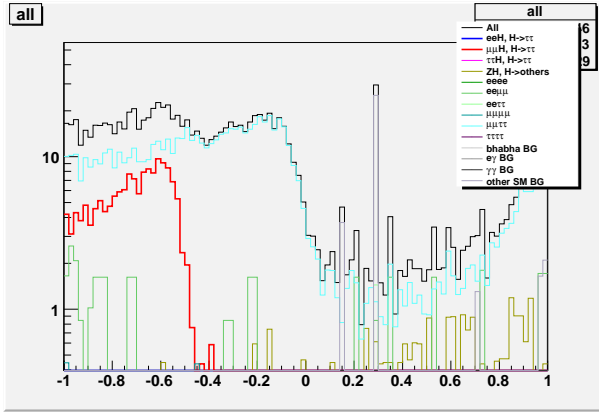


Figure 35:  $\cos \theta_{\tau^+\tau^-} < -0.5$ .

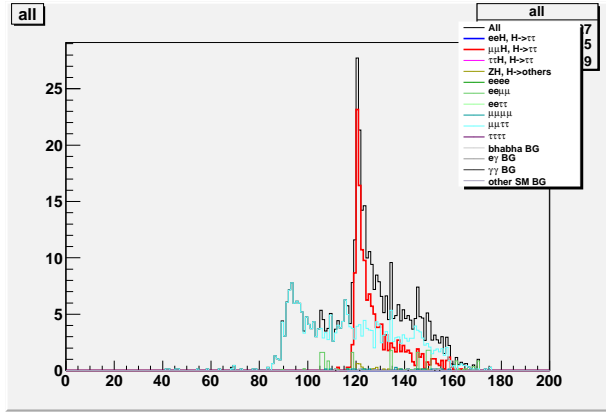


Figure 36:  $118 \text{ GeV} < M_{\text{recoil}} < 143 \text{ GeV}$ .

### B.3 $Z \rightarrow q\bar{q}$ mode

Figures 37 - 49 show the histograms of cut variables. The blue lines in all histograms show the signal process  $ZH \rightarrow q\bar{q}\tau^+\tau^-$ .

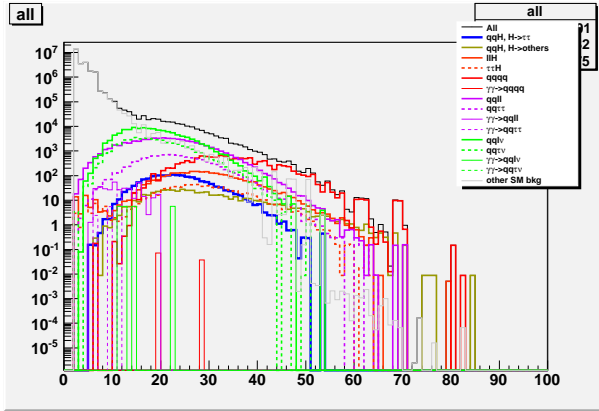


Figure 37:  $9 \leq \text{number of tracks} < 50$ .

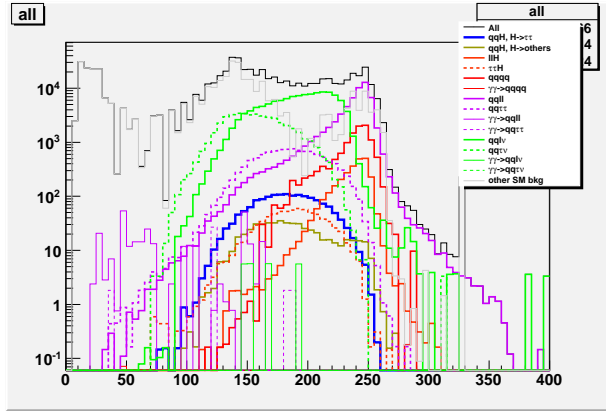


Figure 38:  $110 \text{ GeV} < E_{\text{vis}} < 235 \text{ GeV}$ .

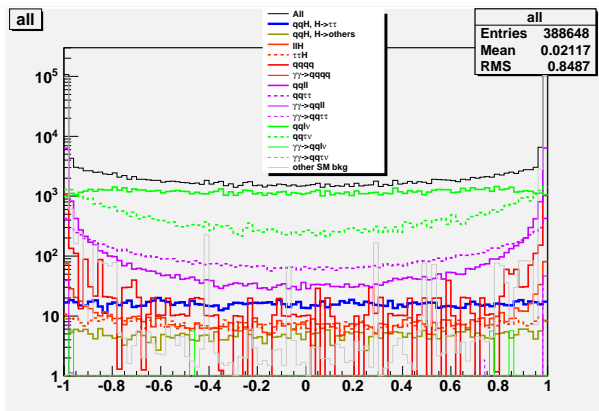


Figure 39:  $|\cos \theta_{\text{miss}}| < 0.98$ .

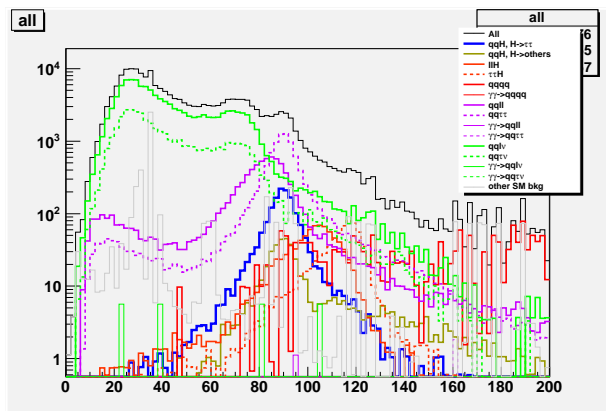


Figure 40:  $77 \text{ GeV} < M_Z < 135 \text{ GeV}$ .

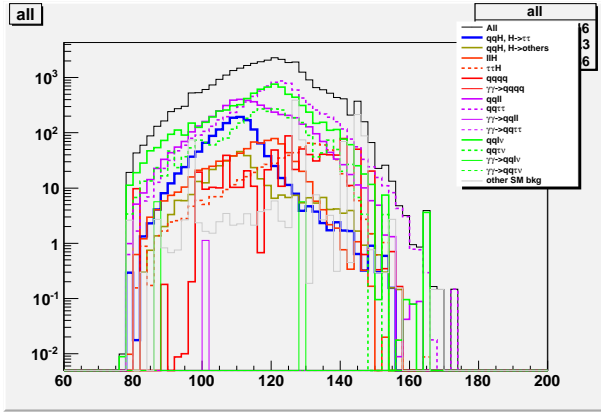


Figure 41:  $80 \text{ GeV} < E_Z < 135 \text{ GeV}$ .

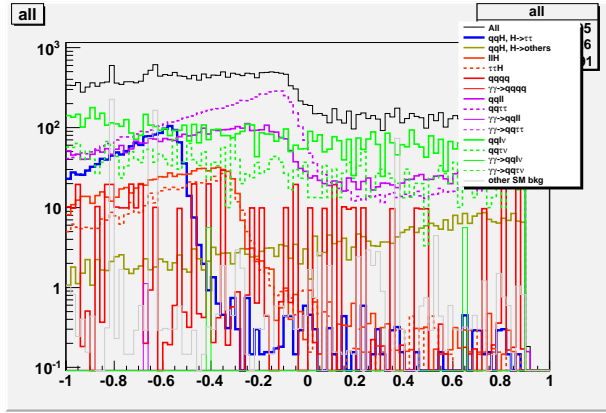


Figure 42:  $\cos \theta_{\tau^+\tau^-} < -0.5$ .

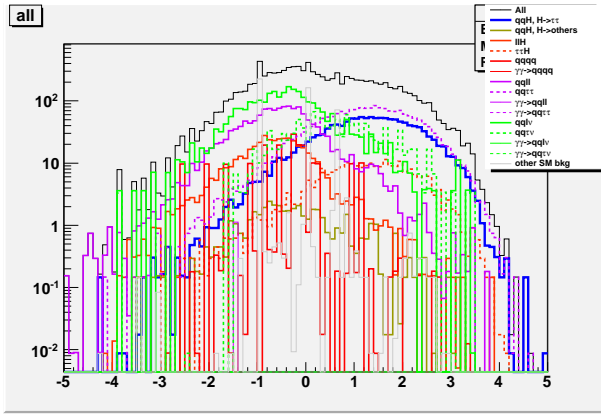


Figure 43:  $\log_{10}(|d_0/\sigma(d_0)|)(\tau^-) > -0.7$ .

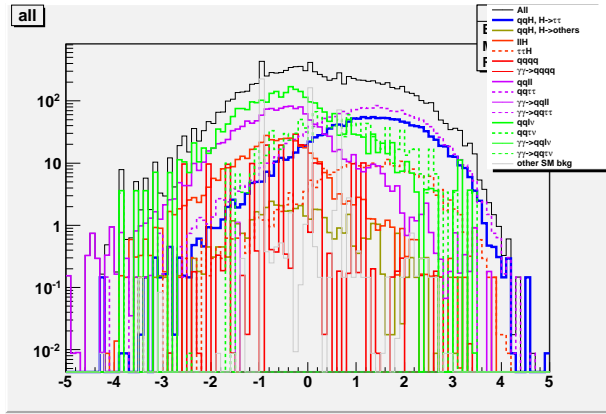


Figure 44:  $\log_{10}(|z_0/\sigma(z_0)|)(\tau^-) > -0.1$ .

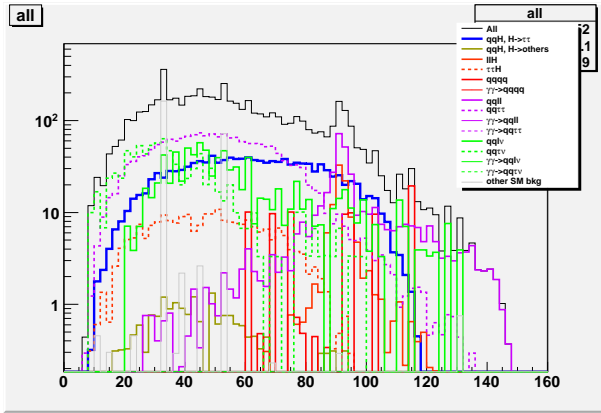


Figure 45:  $M_{\tau^+\tau^-} < 115 \text{ GeV}$ .

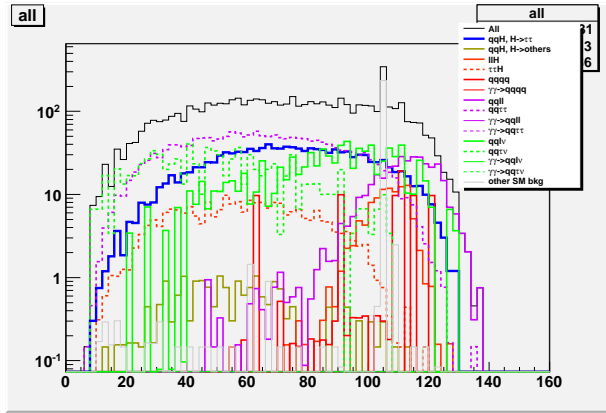


Figure 46:  $E_{\tau^+\tau^-} < 125 \text{ GeV}$ .

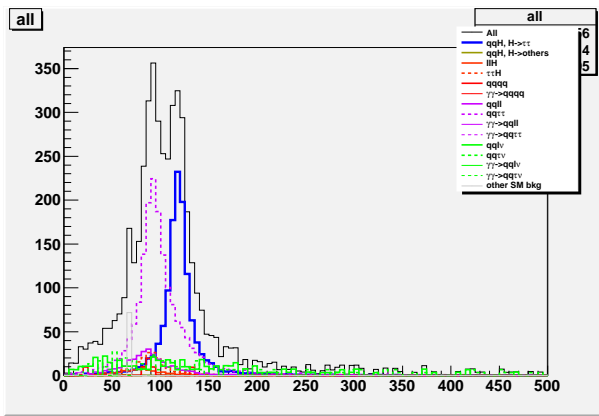


Figure 47:  $100 \text{ GeV} < M_{\text{colapp}} < 170 \text{ GeV}$ .

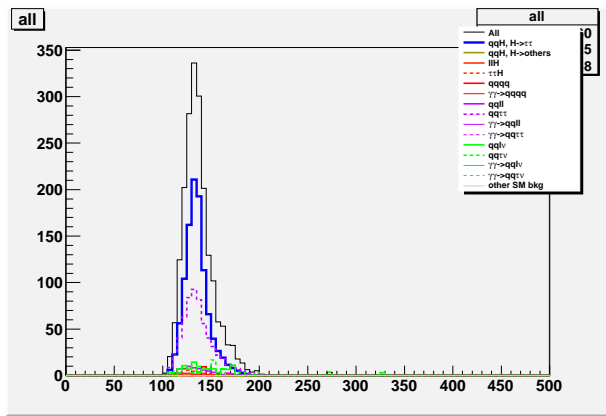


Figure 48:  $100 \text{ GeV} < E_{\text{colapp}} < 280 \text{ GeV}$ .

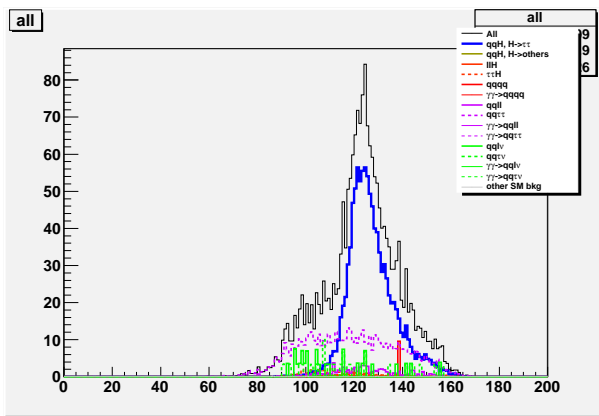


Figure 49:  $112 \text{ GeV} < M_{\text{recoil}} < 160 \text{ GeV}$ .

## References

- [1] The ATLAS Collaboration, "Observation of a new particle in the search for the Standard Model Higgs boson with the ATLAS detector at the LHC", Physics Letters B **716** (2012) 1 - 29
- [2] The CMS Collaboration, "Observation of a new boson at a mass of 125 GeV with the CMS experiment at the LHC", Physics Letters B **716** (2012) 30 - 61
- [3] P. Mora de Fretas, H. Videau, "Detector simulation with Mokka/Geant4 present and future", LC-TOOL-2003-010 (2003)
- [4] <http://geant4.cern.ch/>
- [5] S. Jadach, J. H. Kühn, Z. Was, "TAUOLA — a library of Monte Carlo programs to simulate decays of polarized  $\tau$  leptons", Computer Physics Communications **64** (1991) 275 - 299
- [6] The ILD concept group, "International Large Detector — Letter of Intent" (2010)
- [7] <http://ilcsoft.desy.de/portal>
- [8] T. Sjöstrand, S. Mrenna, P. Skands, "PYTHIA 6.4 physics and manual", Journal of High Energy Physics 0605, 026 (2006)

- [9] LHC Higgs Cross Section Working Group, "Handbook of LHC Higgs Cross Sections: 2. Differential Distributions", arXiv:1201.3084v1 [hep-ph]
- [10] R. K. Ellis, I. Hinchliffe, M. Soldate, J. J. van der bij, "Higgs decay to  $\tau^+\tau^-$  A possible signature of intermediate mass Higgs bosons at high energy hadron colliders", Nuclear Physics B **297** (1988) 221 - 243
- [11] S. Catani, Y. L. Dokshitzer, M. Olsson, G. Turnock, B. R. Webber, "New clustering algorithm for multijet cross sections in  $e^+e^-$  annihilation", Physics Letters B **269** (1991) 432 - 438